Interplay Between KRAS and LZTR1 Protein Turnover, Controlled by CUL3/LZTR1 E3 Ubiquitin Ligase, is Disrupted by KRAS Mutations

Andreas Damianou[1,5,6], Zhu Liang [1,2,5], Frederik Lassen[1,3], George Vere[4], Svenja Hester[1], Philip D Charles[1,2], Adan Pinto-Fernandez[1,2], Alberto Santos-Delgado[3], Roman Fischer[1,2] and Benedikt M Kessler[1,2,6]

[1]Target Discovery Institute, Centre for Medicines Discovery, Nuffield Department of Medicine, University of Oxford, Roosevelt Drive, Oxford OX3 7FZ, UK

[2]Chinese Academy for Medical Sciences Oxford Institute, Nuffield Department of Medicine, University of Oxford, Roosevelt Drive, Oxford OX3 7FZ, UK

[3]Big Data Institute, Nuffield Department of Medicine, University of Oxford, Roosevelt Drive, Oxford OX3 7FZ, UK

[4]Present address: MRC Medical Centre for Medical Mycology, University of Exeter, Geoffrey Pope Building, Stocker Road, Exeter EX4 4QD, UK

[5]Equal contribution

Running title: KRAS activation mutants disrupt CUL3/LZTR1 E3 ligase-controlled turnover

[6]Corresponding authors:

Andreas Damianou
Benedikt Kessler
TDI, CAMS-COI, CMD
Nuffield Department of Medicine
University of Oxford
Roosevelt Drive
Oxford OX3 7FZ, UK
andreas.damianou@ndm.ox.ac.uk
benedikt.kessler@ndm.ox.ac.uk

ABSTRACT (150 words)

KRAS is a proto-oncogene encoding a small GTPase. Mutations contribute up to 30% of human solid tumours including lung adenocarcinoma, pancreatic and colorectal carcinomas. Most KRAS activating mutations interfere with GTP hydrolysis, essential for its role as a molecular switch, leading to alterations in their molecular environment and oncogenic signalling. Here, APEX-2 proximity labelling was used to profile the molecular environment of wild type and G12D, G13D and Q61H activating mutants of KRAS under both, starvation and stimulation conditions. We demonstrate by quantitative proteomics the presence of known interactors of KRAS including a-RAF and LZTR1, which varied in abundance with wildtype and KRAS mutants. Notably, the KRAS mutations G12D, G13D and Q61H abrogate association with LZTR1. Wildtype KRAS and LZTR1, as part of the CUL3 ubiquitin E3 ligase complex, affect each other's protein stability, revealing a direct feedback loop mechanism. KRAS mutations disconnect this regulatory circuit, thereby contributing to oncogenesis.

INTRODUCTION

Kirsten rat sarcoma virus (KRAS) is a signal transducing proto-oncogene that belongs to the superfamily of small GTPases ***(Gimple and Wang, 2019)***. KRAS and other RAS family proteins are molecular switches that alternate between an active and inactive conformational state, determined by its binding to GTP or GDP respectively. Upon environmental stimuli, such as GF mediated signalling, guanine nucleotide-exchange factors (GEF's), including RASGEF1A and RASGRF2 are recruited to facilitate the exchange of GDP to GTP, leading to activation of KRAS ***(Buday and Downward, 1993) (Vigil et al., 2010)*.** Active KRAS promotes signal transduction through effectors such as RAF ***(Moodie et al., 1993)***, TIAM1 ***(Lambert et al., 2002)*** and PI3K ***(Castellano and Downward, 2010)*** and persists until GTP is hydrolysed to GDP, which is catalysed by KRAS-associated GTPase-activating proteins (GAPs).

A balanced equilibrium exists between active and inactive RAS, including KRAS, HRAS and NRAS. In healthy mammalian cells, this can be disrupted by activating point mutations in KRAS, leading to neoplastic properties ***(Prior et al., 2012)***. These mutations activate chronic KRAS signalling, either by impairing GTPase activity and/or the ability of KRAS to interact with negative regulators ***(Liu et al., 2019)***. Subsequent constitutive activation of pro-neoplastic signalling leads to uncontrolled cell division and malignant transformation ***(Haigis, 2017)***.

Despite these detailed insights into KRAS as a GTPase, its turnover and mutation driven effects on KRAS interactors remain incompletely understood. Proximity labelling techniques, such as BioID, TurboID and ascorbate peroxidase 2 (APEX-2), developed recently to capture of protein-protein interactions as well as the exploration of different molecular and cellular environmental 'proximitome' ***(Trinkle-Mulcahy, 2019)***, were applied to wildtype KRAS. For instance, a BioID study investigated the interactome of KRAS, unravelling mTORC2 as a direct KRAS effector ***(Kovalski et al., 2019)*** as well as LZTR1, a ubiquitin E3 ligase adaptor ***(Bigenzahn et al., 2018)***. LZTR1, as part of the CUL3 E3 ligase

complex, was demonstrated to ubiquitinate HRAS at position K170, which consequently alters its cellular localisation by attenuating the interaction of HRAS with the membrane ***(Steklov et al., 2018)***. Additionally, LZTR1 inactivation can lead to a decrease in KRAS ubiquitination, which promotes localisation of KRAS to the plasma membrane ***(Bigenzahn et al., 2018)***. Both reports suggest that LZTR1 affects KRAS function via a non-degradative ubiquitination mechanism. In addition, LZTR1 was proposed also to function also as a "Ras killer protein" by inducing polyubiquitination and degradation of endogenous RAS via the ubiquitin-proteasome pathway ***(Abe et al., 2020)***. An additional level of regulation was revealed by KRAS mono-ubiquitylation at K104, which restores GEF-mediated nucleotide exchange ***(Yin et al., 2020)*.**

Whereas previous studies have predominantly focused on wildtype KRAS, we wondered how oncogenic mutations may affect dynamic proximal molecular interactions. To this end, we applied APEX-2, a rapid proximity labelling approach, to compare interactomes of wildtype KRAS with three mutants G12D, G13D and Q61H upon starvation and/or acute stimulation by exposure to foetal calf serum (FCS) to reveal dynamic interactions of active and inactive forms. Quantitative mass spectrometry analysis confirmed known KRAS interactors such as RAF as well as LZTR1. Strikingly, the wildtype KRAS proximal proteome was altered strongly between the starvation (GDP-bound form) versus the FCS induced (GTP-bound), a trait that was less pronounced with mutants. When comparing the proximal proteome of wildtype KRAS with three different constitutively active mutants, LZTR1 was one of the most predominant proteins preferentially interacting with wildtype but not the mutants. Biochemical studies uncovered that wildtype KRAS and LZTR1, as part of the CUL3 ubiquitin E3 ligase complex, affect each other's protein stability, revealing a direct feedback loop mechanism. KRAS activation mutations appear to disconnect this regulatory circuit, reflecting a possible contribution to tumorigenesis.

MATERIALS AND METHODS

Cell lines

Flp-In™ T-REx™ 293 Cell Line (parental line; R78007, ThermoFisher UK) were cultured in D-MEM™ (high glucose, Gibco #12440-53) supplemented with 10% FBS (Gibco #10500-64), 2 mM L-glutamine (G7513, Sigma-Aldrich), 100 µg/mL Zeocin™ (InvivoGen, ant-zn-1) 15 µg/mL blasticidin (InvivoGen, ant-bl-1) at 37 °C in a humidified 5% CO_2 atmosphere. The stable transfected Flp-In™ T-REx™ 293 Cell Lines (KRas WT-APEX2, KRas G12D -APEX2, KRas G13D -APEX2, KRas Q61H –APEX2, KRas WT-GFP, KRas G12D -GFP, KRas G13D -GFP, KRas Q61H –GFP, GFP only) were cultured in the same medium and selected by adding 100 µg/ml of hygromycin B (InvivoGen, ant-hg-1) to the media. For the induction of the stable transfected Flp-In™ T-REx™ 293 Cell Lines Cells 1µg/mL tetracycline was added to the media.

Plasmids

Q5® High-Fidelity DNA Polymerase (NEB, M0491S) was used to perform PCR reactions following the manufacturer's instructions. APEX2 plasmid was donated from Pedro Carvalho's lab (pcDNA3 APEX2-NES). APEX2 ORF was then PCR amplified and inserted into pcDNA™5/FRT Vector (Invitrogen™) using NEBuilder® HiFi DNA Assembly (NEB, E5520S) following the manufacturer's protocol. KRAS ORF was initially codon optimised and synthesized from Eurofins Scientific. Then KRAS ORF was PCR amplified and cloned into the pcDNA™5/FRT Vector APEX-2 plasmid using NEBuilder® HiFi DNA Assembly following protocol. Different KRAS mutants were generated using Q5® Site-Directed Mutagenesis Kit (NEB, E0554S). The successful clones were confirmed using DNA sequencing.

A pcDNA5/FRT/TO GFP (ITEM 19444) was purchased from Addgene. PCR was used to amplify all the different KRAS (WT, G12D, G13D, Q61H) ORF as well as the pcDNA5/FRT/TO GFP. NEBuilder® HiFi DNA Assembly was used to generate the GFP tagged plasmids. The successful plasmids were confirmed using DNA sequencing.

pcDNA3.1+ Flag-Kras-G12C was a kind gift from Dr Vikram Rao (Pfizer). WT, G12D, G13D and Q61H KRAS were generated using Q5® Site-Directed Mutagenesis Kit. The successful clones were confirmed using DNA sequencing. LZTR1 ORF and the pCI-backbone (Addgene, 41552) were PCR amplified and cloned using NEBuilder® HiFi DNA Assembly.

Immunoblotting

5×10^6 HEK293T or HEK293 FRT were washed with ice-cold PBS and lysed with RIPA buffer containing protease and phosphatase inhibitors. For immunoblotting, 25 µg of protein was then fractionated on Tris–glycine SDS-PAGE gradient (4–15% acrylamide) gels (BioRad; #3450123), transferred onto nitrocellulose membranes (Millipore), and detected with the indicated antibodies using a LI-COR detection system. Primary antibody used in this study: DYKDDDDK Tag Antibody (Flag, Cell Signaling Technology, 2368), A-Raf Antibody (Cell Signaling Technology, 4432), LZTR1 (Santa Cruz Biotechnology, sc-390166), p44/42 MAPK (Erk1/2) (Cell Signaling Technology, 9107), Phospho-p44/42 MAPK (Erk1/2) (Thr202/Tyr204) (Cell Signaling Technology, 4370) GAPDH (Sigma-Aldrich, G8795).

Generation of Stable cell lines

Flp-In™ T-REx™ 293 Cell Line (Invitrogen™) was transfected using Lipofectamine LTX following the manufacturer's protocol. 300 µg/ml of hygromycin B was added the next day and cells were incubated for 2 weeks while medium was changed every 4 days. Finally, the successful population of cells was further used for the described experiments.

Proximity Labelling

5×10^6 HEK293 FRT were induced with 1 µg/mL tetracycline overnight. The next day cells were incubated with 500 µM of Biotinyl tyramide for 30 minutes. A final concentration of 1 mM H_2O_2 was added for 40 seconds. The cells were then washed 2 times with quencher buffer (10 mM sodium ascorbate, 10 mM sodium azide, 5 mM Trolox), 2 times with ice-cold PBS and finally with quencher

buffer for a last time. The cells were lysed with RIPA buffer containing 1 mM PMSF, 5 mM Trolox, 10 mM Sodium Azide, 10 mM sodium ascorbate, protease and phosphatase inhibitors.

Transient Transfection

For DNA plasmids: 5×10^6 HEK293T cells were grown in 6-well plates and Lipofectamine™ 3000 Transfection Reagent (L3000001, ThermoFisher UK) was used to transfect the cells following the manufacturer's instructions. The concentration of plasmids used was indicated in each experiment.

For siRNA transfection experiments: HEK293 cells were grown in 6-well plates and RNAimax transfection reagent (Invitrogen #13778-150) was used following the manufacturer's protocol. A final concentration of 10 nM of the following siRNAs were used: LZTR1 siRNA on-TARGET plus SMARTpool (Dharmacon, L-012318-00-0005) and CUL3 siRNA on-TARGET plus SMARTpool (Dharmacon, L-010224-00-0005).

Cycloheximide chase experiment

5×10^6 HEK293T and HEK293 FRT were transfected with the indicated plasmids for 24 hours. A fresh medium was added for an additional 24 hours and then 50 µg/mL cycloheximide (CHX) was added. Western blot was used to evaluate different expression of proteins.

RAS activation kit

5×10^6 HEK293 FRT were incubated with or without FCS for the indicated time. Cells were then washed with ice-cold PBS and lysed with the designated lysis buffer provided by the active Ras detection kit. Subsequent steps were performed as per the manufacturer's protocol of the active Ras detection kit (Cell Signaling Technology, 8821).

Live Cell Imaging

10,000 HEK293 FRT were seeded in 96 well plates (M33089, ThermoFisher UK) and induced with tetracycline for 24 hours. The next day cells were transfected with LZTR1 siRNA or Control siRNA. 72

hours later we removed the medium. Hoechst 33342 (H3570, ThermoFisher UK) was diluted in PBS in 1:2000 dilution and added to the cells. The cells were then incubated for 10 minutes in the incubator. Cells were imaged using the Opera Phenix microscope. Images were further analysed in Columbus Image Data Storage and Analysis System. The media Cell fluorescent per mean fluorescent per well was then determined for each condition. Finally, the siRNA control was used to normalize the data. The experiment was performed in biological triplicate, and the graph was generated using Prism software (GraphPad Prism 9.2.0).

Sucrose gradient fractionation

HEK293 FRT cells were homogenized in isotonic buffer (0.25 M sucrose, 10 mM Tris-HCl, pH 7,5, 10 mM KCl, 1.5 mM $MgCl_2$, and protease inhibitor cocktail). After homogenization, whole cell lysates were centrifuged at 10,000 g for 10 min to obtain the crude membranes. P10 Crude membranes whereas washed once with the same isotonic buffer and resuspended in the same buffer. 60% and 20% sucrose solutions were prepared in low salt buffer (10 mM Tris-HCl, pH 7.5, 10 mM KCl, 1.5 mM $MgCl_2$) and a continuous sucrose gradient was generated using BIOCOMP Model 108 GRAGIENT MASTER according to manufacturer's guidance. P10 Crude membranes was then loaded on top of the gradient and centrifuged at 170,000 g for 2 hrs. 12 fractions (500 µl1 mL per fraction) were collected from top to bottom.

Membrane-cytoplasmic cellular fractionation

Fresh HEK293 FRT cell pellets were suspended in digitonin lysis buffer (50 mM HEPES pH 7.5, 10 mg/mL digitonin, 150 mM NaCl) and incubated for 30 minutes in $4^{o}C$ under spinning. The sample was spun at 6000xg for 5 min in 4 ^{o}C. The supernatant (cytoplasmic fraction) was moved to a new tube. The pellet was re-suspended in 0.3 % NP-40, 50 mM HEPES pH 7.5 and 150 mM NaCl and incubated on ice for 5 min. The samples were centrifuged at 1500 g for 5 minutes. The supernatant (membrane fraction) was transfer to a new tube and stored at -20 ^{o}C until analysis.

Streptavidin immunoprecipitation

For immunoprecipitation (IP) experiments, Dynabeads™ MyOne™ Streptavidin T1 for western blot 30 µL was used and for mass spectrometry 110 µL. Initially the beads were washed twice with RIPA buffer once with 1M KCL, 0.1 M Na_2CO_3 and 2 M Urea in 10 mM Tris-HCL, pH 8 and finally twice with RIPA buffer again. For Western blot biotinylated proteins were eluted using 60 µL of 2X loading buffer supplemented with 2 mM biotin and 20 mM DTT by boiling (98 ^oC) for 10 minutes. For Mass spectrometry, an on bead-based digestion protocol was used as described below.

On-beads digestion and mass spectrometry sample preparation

Immunoprecipitated protein samples were denatured in 8 M Urea in 100 mM triethylammonium bicarbonate buffer (TEAB) for 30 minutes at room temperature. Afterwards, the samples were reduced with 10mM tris(2-carboxyethyl)phosphine (TCEP) for additional 30 minutes at room temperature. 50 mM iodoacetamide was added to the sample for 30 minutes at room temperature to alkylate the proteins. Samples were then diluted down to 1.5 M Urea with 50 mM TEAB. Finally, 250 ng dissolved in 50 mM TEAB and incubated in 37 ^oC overnight. The next day samples were desalted using a C18 solid phase cartridge (Sep-Pak, Waters) following the manufacturer's protocol. Purified peptide eluates were dried by vacuum centrifugation and re-suspended in buffer A (98 % MilliQ-H_20, 2 % CH_3CN and 0.1 % trifluoroacetic acid - TFA) and stored at -20 ^oC until analysis.

Liquid chromatography-tandem mass spectrometry (LC-MS/MS) analysis

LC-MS/MS analysis was performed essentially as described previously ***(Fischer and Kessler, 2015)***. In brief, resuspended peptide material was trapped on an Acclaim™PepMap™ 100 C18 HPLC Column (PepMapC18; 300 µm x 5 mm, 5 µm particle size, Thermo Fischer) using solvent A (98 % MilliQ-H20, 2 % CH3CN and 0.1 % TFA) at a pressure of 60 bar and separated on an Ultimate 3000UHPLC system (Thermo Fischer Scientific) coupled to a QExactive mass spectrometer (Thermo Fischer Scientific). The peptides were separated on an Easy Spray PepMap RSLC column (75 µm i.d. x 2 µm x50 mm, 100 Å,

Thermo Fisher) and then electrosprayed directly into an QExactive mass spectrometer (Thermo Fischer Scientific) through an EASY-Spray nano-electrospray ion source (Thermo Fischer Scientific) using a linear gradient (length: 60 minutes, 5 % to 35 % solvent B (0.1 % formic acid in acetonitrile), flow rate: 250 nL/min). The raw data was acquired on the mass spectrometer in a data-dependent mode (DDA). Full scan MS spectra were acquired in the Orbitrap (scan range 380-1800 m/z resolution 70000, AGC target 3e6, maximum injection time 100 ms). After the MS scans, the 15 most intense peaks were selected for HCD fragmentation at 28 % of normalised collision energy. HCD spectra were also acquired in the Orbitrap (resolution 17500, AGC target 1e5, maximum injection time128 ms) with first fixed mass at 100 m/z.

Proteomic data analysis

Raw mass spectrometry (MS) data was processed using MaxQuant software (v1.6.14.0) and searched against human protein sequences in UniProt/KB (version). For data analysis, Perseus (version 1.6.15.0) and Significance Analysis of INTeractome (SAINT) workflows ***(Choi et al., 2012)*** were applied. The MS data generated in this study has been submitted to the PRIDE public repository with the accession number PXD029725.

Data analysis

We characterized differentially enriched proteins in G12, G13 and Q61H mutants versus wildtype during starvation and FCS. To do this, we first used Perseus (version 1.6.15.0) to perform a student's t-test to evaluate Log Fold Changes (Log2 FC) between wildtype and mutants. For each condition, we then carried forward the differentially expressed proteins with a log2(mutant/WT FC) > 0.5 or < -0.5 and - log10 (p value) > 1.3. Proteins that fulfilled the above filtering criteria were considered to be potential mutant- or wildtype KRAS-specific interacting proteins. Gene ontology enrichment analysis of differential proximal proteins for three mutants were performed using the Metascape web-based tool (www.metascape.org) ***(Zhou et al., 2019)***. To further investigate if KRAS mutants G12D, G13D and

Q61H differ in downstream signalling pathways and known interactors, we compared the protein components in different pathways (MEK-RAF, mTOR, PI3K, RALGDS, RASSF, and TIAM-RAC) and known KRAS interacting partners enriched with different mutants and wildtype KRAS. Protein abundance was shown as Log2 (LFQ) value in the heatmap shown in **Fig 3E**.

We also investigated the overlap between our significantly enriched proteins (log2 [mutant/WT FC] > 0.5 or < -0.5 and - log10 [p value] > 0.8) and various gene sets including i) GO molecular function, ii) GO biological processes iii) GO cellular compartments and iv) MSigDB Hallmark genes and v) CORUM complexes ***(Giurgiu et al., 2019)***. To do this, we used Genoppi ***(Pintacuda et al., 2021)*** to perform a one-tailed hypergeometric overlap test to assess the probability of finding a given gene set among our significantly enriched proteins. We performed two different analyses. First, we performed a "global analysis", where we assess the overlap of gene sets in interactors compared to other genes in the genome. Second, we performed a "conditional analysis" where we assess the overlap of gene sets in interactors compared to other proteins found in the experiment.

Software developed for data analytics

All analyses were performed with R version 4.0.2. Workflows and scripts have been compiled in a custom R-package that can be found in the following repository https://github.com/frhl/KRAS-methods.

RESULTS

KRAS-APEX-2 wildtype, G12D, G13D and Q61H mutants express, localise and function similarly to endogenous KRAS

To comprehensively characterize the proximal proteome of wildtype (WT) KRAS and of three of the most frequent oncogenic driver mutants (G12D, G13D and Q61H), we adapted an APEX2-dependent proximity labelling method **(Fig. 1A)**. To this end, we first generated tetracycline-inducible stable cell lines to minimize KRAS misfolding and mislocalization. Also, the same parental cell line was used as a control to generate a 'benchmark' proteome, enabling an unbiased comparison. Four different HEK293 FRT T-Rex cell lines (KRAS WT, G12D, G13D and Q61H) expressing WT KRAS- and all mutants-APEX2 fusion proteins in a stable fashion upon treatment with tetracycline **(Fig. 1B)** were generated. Furthermore, to examine the activity of APEX2 within the expressed constructs, streptavidin blot analysis and immunofluorescence were used to test its in-cell biotinylation ability. In the presence of tetracycline, phenol biotin and H_2O_2, biotinylated proteins are detected as a wide band pattern, whereas just three endogenous biotinylated protein bands observed in all negative controls, indicating highly specific APEX2 labelling **(Fig. S1A)**.

APEX-2 tagging may interfere with cellular localisation, signal transduction and GTP hydrolysis. To test this, the four cell lines were starved for 2 and 4 hours, respectively, and ERK/phospho-(p)-ERK activation was tested. As expected, upon starvation, pERK levels were reduced in WT KRAS, but not the mutants **(Fig. 1B)**. GTP-KRAS levels, measured using GST-Raf1-RBD enrichment, were decreased upon starvation only in the WT, but not in the constitutively active KRAS mutants, indicating that APEX-2 does not interfere with these processes **(Fig. 1B)**. KRAS-APEX-2 fusion protein expression was further examined for its localisation. To this end, T-Rex tetracycline inducible lines expressing GFP-KRAS fusion protein and GFP only were generated (**Fig. S1B**). Microscopy analysis indicated the correct localisation of GFP-KRAS on the plasma membrane, whereas GFP only was located in the cytosol **(Fig. S1B)**.

Residual nuclear localisation was noted in less than 10% of the cells **(Fig. S1C)**. To complement this, subcellular fractionation was used to separate membranes from cytoplasmic fractions, confirming the localisation of KRAS-GFP and GFP only as observed by microscopy (data not shown). Also, the KRAS-APEX-2 WT and mutant fusion proteins were enriched in the membrane fraction **(Fig. S1D)**. We also examined the ability of KRAS-APEX2 fusion proteins to translocate upon starvation and FCS stimulation as their endogenous counterpart does. A Sucrose gradient fractionation experiment revealed similar translocation and localisation profiles for KRAS-APEX-2 fusion protein and endogenous KRAS upon 10 min FCS stimulation, 15 hours after initial starvation. Most importantly, APEX-2 labelling took place within the correct subcellular environment where endogenous KRAS is located **(Fig. S1E)**. Together, we conclude that KRAS-APEX-2 fusion proteins showed similar functional properties as compared to endogenous KRAS.

APEX-2 labelling reveals differential molecular environments between WT and KRAS mutants

Proximity labelling experiments were conducted with APEX2-KRAS WT, G12D, G13D and Q61H expressing cell lines to compare their molecular vicinities. As controls, the APEX2-KRAS WT expressing cell line was analysed with and without tetracycline induction. We used a “beads only” background control as KRAS itself is expressed in different locations, thereby complicating analysis. In each case, we compared starvation and 10 min FCS induction. Tetracycline induction was performed overnight for a sufficient expression of the bait, followed by incubation in presence or absence of FCS for 15 hours **(Fig. 1C)**. Protein biotinylation was observed only in the presence of tetracycline, and the Raf/MEK/ERK pathway was not active during starvation of the WT, but not for the cells expressing oncogenic mutants (**Fig. 1D**).

Proximity labelled biotinylated material was isolated, digested and analysed by quantitative mass spectrometry. MS data were further processed with an interaction scoring algorithm SAINTexpress ***(Teo et al., 2014)*** to establish interaction probabilities (true proximity proteins) with KRAS baits under

different conditions. A Saint Score above 0.8 with >=4- fold enrichment yielded 700-1000 KRAS proximal proteins per condition and a total of 1,373 proteins identified **(Fig. 2A,B)**.

First, KRAS interacting partners were divided into several categories including receptors, activators, repressors, interactors and canonical RAS effectors proteins ***(Kiel et al., 2021)***. Additionally, to "benchmark" our results, the BioGRID (https://thebiogrid.org/) database was used to retrieve the previously known KRAS 'proximitome' ***(Adhikari and Counter, 2018; Bigenzahn et al., 2018)***. We detected proteins associated with KRAS signal transduction (Receptor Tyrosine Kinases (RTKs) including EGFR, MET and ERBB2IP), eight Ras effectors (RAF1, a-RAF1, TIAM1, RAPH1, RAPGEF2, RAPGEF2, SNX27 and MYO10). Also, several known KRAS interactors, activators and repressors were identified in our experiment including the E3 ligase adaptor protein LZTR1, DAG1 and GRB2 **(Fig. 2B)**. We also captured several proteins found to be part of downstream KRAS signalling, including proteins taking part in the networks of MEK-Raf (3 proteins), PIK3 (8) mTOR (2), TIAM RAC (3), RALGDS (8) and RASSF pathways (1) **(Fig.2 B).**

206 out of the 1,373 proximal proteins identified were shared between our study and previous BioID proximal studies **(Fig. 2B)**. 313 proteins were common between conditions and many hits unique to the different KRAS species **(Fig. 2C)**. APEX2 proximity labelling efficiency is reflected by the capture of low abundance proteins, not readily present in HEK293 deep proteome data sets ***(Geiger et al., 2012)***. For instance, we captured several low abundant canonical KRAS 'interactors', such as RAF, TIAM1, SNX27, MARK2, demonstrating effective APEX2-based enrichment **(Fig. 2D)**.

Despite stringent threshold criteria, 1,373 identified proteins remained after the first pass, requiring further filtering approaches for the confident discovery of novel KRAS 'proximitome' candidates. A major hallmark revealed by our experiment, different from previous studies, was how the oncogenic mutations G12D, G13D and Q61H, located in the KRAS G domain, perturbed the KRAS molecular environment. For instance, in contrast to WT KRAS, RAF1 and ARAF were enriched with G12D, G13D

and Q61H in both starvation and FCS stimulation **(Fig S3A-S3F)**, suggesting that the RAF-MEK-ERK pathway is highly activated in theses mutants, consistent with the ERK phosphorylation status **(Fig 1D)** and previous studies ***(Haigis, 2017)***. It is noted that, not only the mutations but also the expression level can affect protein-protein interaction (PPI) networks. Therefore, the enhanced interaction between ARAF, RAF1 and KRAS mutants may also be caused by high expression. Furthermore, NF1 and SPRED2 are only enriched with the G13D and Q61H mutants, but not with G12D, suggesting that G13D and Q61H are associated with NF1/SPRED2 to a greater extent as compared to G12D, consistent with previous findings reporting that NF1 is not able to affect G12D KRAS ***(Rabara et al., 2019)***. Notably, we found that LZTR1, an essential regulator for KRAS ubiquitination and degradation, was less abundant in all three mutant KRAS proximal proteomes, suggesting a decreased interacting affinity with mutant KRAS.

To further investigate the pathways that are selectively ascribed to or shared between the proximal proteins enriched in three different mutants, under resting or FCS stimulation conditions, we performed network enrichment analysis and visualization using Metascape **(Fig. 3A-3B)**. The network shows that processes such as Rho GTPase signalling, actin filament-based process, and cell morphogenesis were clustered and shared between resting and FCS stimulation conditions. Under the resting condition, pathway clusters such as cellular amino acids metabolism, actin filament-based process, are mostly shared between the G13D and Q61H mutants, indicating that the mutations potentially affect KRAS function via perturbations in proximal protein networks. In contrast, under FCS stimulation condition, most of the pathway clusters are shared among all three mutants, suggesting less mutant-specific effects.

We also examinded changes between the 'proximitome' of the three KRAS mutants, especially in the newly identified proteins as well as the subset of hits that have previously reported in other proximity KRAS studies. We observed stronger association of mTOR, with all the three mutants as compared to the wild type, as expected. Interestingly, a stronger association with WT as compared to mutants was

observed with NF2, a possible negative regulator of KRAS signalling (Cui et al.,2019). Several 'proximitome' hits seem to have a preference toward a specific KRAS mutants such as VPS45 (G12D FCS), ACSL4 (Q61H ST) VAMP3 (G13D ST) and ROCK2 (G13D and Q61H) **(Fig 3C)**. VAMP3 as part of SNARE complex was previously reported to regulate KRAS membrane localisation, identified to interact equally when we compare WT Vs G12D and Q61H **(Fig 3C)**. Nevertheless, during starvation, the G13D mutant seem to dramatically decrease its interaction with VAMP3 **(Fig 3C)**.

Any proteins that were not previously reported as a known KRAS proximitome or interactome were considered as novel KRAS proximal proteins. 26 were found to be enriched in one out of the three KRAS mutants as compared to wild type **(Fig 3D)**. Several of those proteins show a preference toward a specific KRAS mutant **(Fig 3D)**.

LZTR1 differently affects wildtype versus KRAS mutants

This prompted us to perform a systematic search for KRAS associated partners with a different mutant associated abundance profile in our data set. Canonical and non-canonical interactors (including effectors, activators, repressors and receptors) were selected and visualised **(Fig 4A)**. Among the 105 previously reported physical interactors, 22 were identified here. Of these, LZTR1, ARAF, RAF1 and NF1 showed different abundance profiles between WT and mutant KRAS. Most notably, LZTR1 showed a weaker abundance associated with oncogenic G12D, G13D and Q61H KRAS mutants as compared to wildtype (Fig 4A). To test the preference of LZTR1 to be preferentially enriched with WT KRAS over the mutants, an APEX-2 labelling experiment was performed with Western blotting as a readout. Indeed, LZTR1 was detected in all samples except the beads control and enriched in the WT versus the mutants. ARAF was used as a control reflected by an enriched profile associated with KRAS mutants **(Fig. 4B)**.

LZTR1 controlled KRAS protein turnover is altered by oncogenic KRAS mutants

The enrichment of LZTR1t in the proximal proteome of WT KRAS related to the mutants might be linked to differential protein turnover. To test this, siRNA knockdown of LZTR1 was performed in HEK293 cells expressing WT KRAS-GFP, G12D-GFP, G13D-GFP and Q61H-GFP fusion proteins. As a control, a GFP only HEK293 FRT cell line was generated. The GFP fluorescent signal was monitored in the different stable cell lines, and the GFP cell line was used to assess the global effect of LZTR1 on protein expression. Knockdown of LZTR1 stabilised WT KRAS GFP expression but not GFP only **(Fig.4C, S5A),** consistent with its role as an adaptor protein to promote ubiquitination of KRAS, resulting its degradation as reported previously ***(Abe et al., 2020)***. Notably, KRAS stability was strongly diminished in the G12D, G13D KRAS and slightly decreased in the Q61H KRAS mutants **(Fig.4C, S5A)**. This suggests that the half-life of oncogenic KRAS mutants might be increased compared to the WT counterpart. To further explore this, KRAS-GFP cell lines expressing WT and oncogenic KRAS mutants (G12D, G13D and Q61H) were treated with cycloheximide (CHX) for different times. We observed a shorter half-life of WT KRAS as compared to the oncogenic mutants **(Fig. 4D, E)**. WT KRAS was strongly depleted after 10 hours of CHX treatment, and the oncogenic mutants more stable **(Fig. 4D, E)**. To further explore whether LZTR1 differently affects KRAS oncogenic mutants, Myc-LZTR1 was co-expressed with 3Flag-KRAS WT, G12D G13D or Q61H. Elevated LZTR1 levels yielded substantially decreased WT KRAS protein levels, whereas the three oncogenic KRAS mutants show little to no protein downregulation. Most notably, LZTR1 protein levels were highly upregulated in the presence of oncogenic KRAS, suggesting a possible interdependence between KRAS and LZTR1 protein levels and turnover **(Fig. 4E)**. To get further insight, we tested how KRAS mutations affect protein stability in the presence of LZTR1 using a cycloheximide (CHX)-chase assay. At the start of the CHX-chase assay, WT KRAS protein levels were much lower as compared to any of the three mutants. In cells co-expressing Flag- KRAS WT and Myc-LZTR1, KRAS protein levels were reduced by half after 12 hours of CHX treatment, whereas the three mutant protein levels were unchanged. Remarkably, LZTR1 levels were also differentially affected in the presence of WT versus mutant KRAS **(Fig. 4G)**. Taken together, these results suggest that KRAS

degradation, occurring in an LZTR1 dependent manner, is altered by oncogenic mutations. In turn, LZTR1 levels are also affected in the presence of WT, but not KRAS mutants.

WT KRAS and LZTR1/CUL3 regulatory circuit disrupted by oncogenic KRAS mutants

LZTR1 was described as a substrate adaptor of CUL3-based ubiquitin E3 ligase ***(Bigenzahn et al., 2018; Hollstein and Cichowski, 2013).*** Therefore, we decided to examine whether the inhibition of NEDD8-activating enzyme (NAE) by inactivation of Cullin-RING E3 ubiquitin Ligases (CRLs) via blocking Cullin neddylation has any effect on KRAS and LZTR1 protein stability. MLN9424 is a newly discovered small molecular inhibitor of NEDD8-activating enzyme (NAE) and it was used as an inhibitor of CRLs ***(Milhollen et al., 2010)***. HEK293 cells were initially co-transfected with LZTR1 and WT or KRAS mutants, followed by treatment with different concentration of MLN9424 for 24 hours. Co-transfection of LZTR1 and WT KRAS reduced KRAS protein levels, which were restored in the presence of MLN9424 **(Fig. 4H)**. This was not observed with the oncogenic KRAS G12D and G13D mutants, perhaps to some extent with Q61H in the presence of high concentrations of MLN9424 (1μM). Notably, LZTR1 protein levels were upregulated with MLN9424, predominantly in presence of WT KRAS. LZTR1 and WT KRAS protein levels showed an interrelated abundance profile not observed with the mutants, perhaps with the exception of KRAS G12D to a minor extent **(Fig. 4H)**.

To study the underlying dynamics of this effect, MLN9424 inhibitor experiments were performed in a time-dependent fashion. HEK293 cells were co-transfected with Myc-LZTR1 and Flag-KRAS. Cells were then incubated with 0.3 μM MLN9424 for 0, 6 and 18 hours, respectively. WT KRAS protein levels were gradually increased, whereas the oncogenic KRAS mutant protein levels remained at a similar level **(Fig. 4I)**. LZTR1 protein levels followed a comparable trend. Once more, only in the presence of the WT KRAS, LZTR1 protein levels were notably increased. A small exception was G12D KRAS, were a minor increased in LZTR1 levels was observed **(Fig. 4I)**. Since Cullin3 was previously shown to regulate (WT) KRAS protein levels via LZTR1 ***(Abe et al., 2020),*** we knocked down Cullin 3 to investigate how

LZTR1 protein levels behaved in the presence of CHX. Removal of Cullin3 led to an increase of LZTR1's protein half-life, suggesting that Cullin 3 regulates its own co-factor (LZTR1) in a substrate (KRAS)-dependent manner **(Fig. S5B)** To further examine how KRAS protein levels affect LZTR1 protein stability, HEK293 cells were co-transfected with LZTR1 and KRAS, where either KRAS **(Fig. S5C)** or LZTR1 plasmid concentration were kept constant **(Fig. S5D)**. In both cases, we observed that LZTR1 protein levels were stabilised in a dose-dependent manner similar to KRAS, indicating a direct crosstalk between KRAS and LZTR1. This appeared to be Cullin3 dependent, because when Cullin 3 was knocked down, Flag-KRAS and Myc-LZTR1 co-expression did not lead to LZTR1 accumulation, whereas Flag-KRAS protein levels were stabilised **(Fig. S5E)**. We conclude that the regulation of KRAS and LZTR1 turnover are linked, possibly involving Cullin Ring Ubiquitin Ligases (CRLs), in particular Cullin 3 (**Fig. 4J**).

DISCUSSION

Oncogenic KRAS G12D G13D and Q61H are amongst the most common point mutations found in human cancer ***(Cook et al., 2021; Liu et al., 2019)***. KRAS mutations appear in different cell types with allele-specific profiles, suggesting different underlying mechanisms behind driving cell transformation. For instance, G12D KRAS mutation is appearing in over 90% of pancreatic ductal adenocarcinoma (PDAC) ***(Wong et al., 2016),*** G13D is most frequent in colon adenocarcinoma ***(Taieb et al., 2017)*** and Q61H in lung adenocarcinoma ***(Kunimasa et al., 2020).*** KRAS-dependent oncogenesis is depended on at least four factors contributing to different KRAS mutations being associated with specific cancer types ***(Prior et al., 2012)***. First, expression levels as well as GTP/GDP-KRAS ratios contribute to cell transformation. Active KRAS dynamics varies considerably between different oncogenic mutations ***(Killoran and Smith, 2019)*** and maybe influenced by alterations in GEF, GAF and effector interactions

***(Kiel et al., 2021)*.** Finally, the genetic, epigenetic and proteomic environment of different cell types differential impact RAS-dependent oncogenesis.

Here, we systematically investigated how these oncogenic driver mutations of KRAS affect their proximal molecular environment. The use of an isogenic cell line as control reduced interference due to different cellular backgrounds. Our approach relied on an over-expression system, and it is known to potentially provoke cell transformation ***(Ito et al., 2021)*.** However, we have carefully controlled this with an optimised starvation protocol to mimic a "baseline state". Of note, we cannot exclude the possibly of missing crucial KRAS associations in our experimental system due to intrinsic limitations of over-expression systems. An APEX-2 proximity labelling was used as it occurs at a timescale of seconds, which is advantageous for the capture of transient interactions as well as fast molecular changes as compared to BioID-based approaches ***(Trinkle-Mulcahy, 2019)***. Labelling conditions were optimised and levels of protein biotinylation assessed in whole cell lysates as well as streptavidin eluate material to control for consistency (**Fig 1D**). Previous proteomics-based studies exploring the KRAS "proximitome", based on BioID, revealed many shared proteins between WT & mutant KRAS (mainly G12V, S17N, C185S), predominantly involved in protein expression and trafficking ***(Kiel et al., 2021; Li et al., 2012; Matallanas et al., 2003)***. Additionally, there appears to be a large overlap between GTP/GDP KRAS interactors (proteins in closed proximity), indicating a more gradual KRAS activation transition rather than being an on/off switch. Very few specific interactors were reported, such as the KRAS G12V selective interaction with phosphatidylinositol-4-phosphate 5-kinase type 1 (PIP5K1), mediating PI3K and ERK signalling ***(Semenas et al., 2014)***.

Our approach offers a deeper insight as APEX2 may capture more concise molecular snapshots, and we systematically compared the molecular environment of WT KRAS compared to G12D, G13D and Q61H mutants, respectively, under resting and acute FCS stimulation conditions. Residues G12, G13 and Q61 are in the KRAS G domain, altering nucleotide binding and exchange and are expected to alter KRAS interacting networks. To further examine the difference in the downstream network, proteins

involved in the known KRAS signalling pathways, the RAF-MEK, mTOR, PI3K, RALGDS, RASSF and TIAM-RAC networks were selected and visualised **(Fig 3G)**. In total, 37 downstream signalling proteins were identified among all the samples, and we did not observe significant differences between WT KRAS and all the mutants. Gene ontology-cellular component analysis for WT and the mutants showed enrichment of focal adhesion and plasma membrane, in line with its subcellular localization **(Fig 3H)** and consistent with previous studies ***(Kiel et al., 2021)*.**

The absence of some canonical Ras interactors, such as b-RAF, H-Ras/N-Ras and SOS, could be explained by the lack of accessible lysine residues for the biotinylation reaction to take place or perhaps the low expression level of some of those proteins in HEK293 cells, as it is the case for b-Raf ***(Geiger et al., 2012)***. A-RAF in turn seems to be strongly enriched with KRAS G13D as compared to G12D and Q61H. On the other hand, NF1 and SPRED2 seem to be enriched to a greater extent with the G13D and Q61H mutants as compared to G12D, in line with previous findings that the G12D KRAS signalling pathway is not affected by NF1 ***(Cheng et al., 2021)***.

As shown previously ***(Bigenzahn et al., 2018; Kovalski et al., 2019)***, LZTR1 was detected in the micro-environment of both WT and selected KRAS mutants. Most notably, we found that LZTR1 levels were strongly reduced in proximity of the mutants, especially G12D, G13D and to a lesser extent with Q61H (**Fig 4A)**. LZTR1's effect on ubiquitination and turnover of WT KRAS and some mutants has been examined (Abe et al., 2020). We extend this observation to the KRAS mutants G12D, G13D and Q61H, whose turnover was less dependent on LZTR1 (**Fig 4D, E**). Importantly, we discovered a reciprocal effect on LZTR1 protein turnover itself that was most prevalent in the presence of WT KRAS (**Fig 4B, D-I**) and CUL3-dependent (**Fig S5C, F**), indicating a direct (WT)-KRAS-LZTR1 regulatory circuit that appears to be disrupted by KRAS mutants (**Fig 4J**). This further demonstrates the interplay between LZTR1, a CUL3 ubiquitin E3 ligase adapter for KRAS. It will be interesting to explore whether LZTR1 mutations, prevalent in Rasopathies such as glioblastoma & dominant Nooan syndrome ***(Motta et al.,***

2019; Steklov et al., 2018), may also affect this molecular regulatory circuit with potential consequences for malignant cell transformation.

FIGURE LEGENDS

Figure 1: KRAS-APEX-2 wildtype, G12D, G13D and Q61H mutants express, localise and function similarly to endogenous KRAS. (A) Schematic representation of the approach used in this study to investigate the proximal proteome of K-Ras. First step is the generation of a fusion K-Ras APEX-2 protein with a flexible linker in between K-Ras and APEX-2. Second step, phenol biotin and H2O2 was added in the media to facilitate the biotinylation of proteins close proximal to the bait including effectors, regulators and interactors of K-Ras as well as proteins located in close proximity with K-Ras. The next step included the IP using streptavidin beads to capture biotinylated proteins. Finally, biotinylated proteins were digested, and mass spectrometry was used to identify proximal proteins. **(B)** Western blot analysis showing ERK, pERK, and a-FLAG in both cell extract and IP (immunoprecipitation) using GST-Raf1-RBD (Activate Ras Detection Kit) 2 and 4 hours upon starvation. As an IP positive control lysate was incubated with GTPγS and for IP negative control lysate was incubated with GDP. (**C**) Experiments were carried out in biological triplicates (n=3). KRAS has a long half-life the absent of tetracycline will decrease the proximal labelling of the new expressed KRAS. For the starvation condition cells were directly move for 30 minutes incubation with phenol biotin and subsequent incubation with H_20_2 for 45 seconds. On the other hand, for the FCS induction condition cells were starver for 15 hours with a subsequent incubation with phenol biotin for 30 minutes. The last 10 minutes additional 20% FCS (including biotin phenol) was added to activate the cells. 45 seconds of H_20_2 was used to initiate the biotinylating of the KRAS proximal proteins. **(D)** Western blot analysis showing ERK, pERK and a-FLAG in cell extract upon APEX-2 labelling under different environmental conditions including starvation and FCS induction. Additionally, western blot analysis indicating biotinylating proteins (Streptavidin, DyLight 488 Conjugated) upon streptavidin-

immunoprecipitation. APEX-2 experiments were carried out in three independent biological experiments.

Figure 2: KRAS wildtype, G12D, G13D and Q61H proximal proteomes

(A) Mass spectrometry data analysis schematic representation. Data were initially analysed MaxQuant to identify proteins presence in our samples. Data were then processed with an interaction scoring algorithm SAINTexpress to provide a score on the probability of a true 'interaction' (true proximity protein) with our bait. Finally, true proximity proteins were decided to include any protein that has SAINT score above 0.8 and fold difference higher or equal to 4 as compared to the beads control. On the other hand, MaxQuant results were further analysed on Perseus and volcano blots were generated. **(B)** All Ras-proximal proteins identified in each APEX-2 KRAS proximitome. SAINTq probability ≥ 0.8; fold change ≥ 4 over beads control (1373 proteins). Several KRAS interactome families (Receptors, Repressors, Activators, Interactors, Classical Ras effectors, Proximitome, MEK-RAF pathway, PIK3 pathway, TIAM-RAC pathway, RALGDS pathway, RASSF pathway) were explored. **(C)** Histogram showing intersection of common protein groups between KRAS species and treatment. **(D)** KRAS proximal landscape (blue - previously known; grey – from this study) from the APEX-2 proximitome (left compartment) relative to the cellular proteome (right compartment). Previously known Ras effectors including activators, repressors and activators are indicated in red.

Figure 3: Enriched proteomes between KRAS wildtype and G12D, G13D and Q61H mutants

(**A-B**) Metascape enrichment network visualization showing the intra-cluster and inter-cluster similarities of enriched terms (up to ten terms per cluster), in starvation (**A**) and FCS stimulation state (**B**) separately, where nodes are represented by pie charts indicating their associations with three different mutants. The colour code for pie sector represents G12D (red), G13D (blue), and Q61H

(green). Cluster labels were added manually. (**C**-**D**) Heatmap showing the log2(FC MUT/WT) of differentially enriched proximal proteins which were reported in previous proximitome studies (**C**) or proposed based on our study (**D**) Asterisk indicates that the hit meets the criteria of log2(mutant/WT FC) > 0.5 or < -0.5 and - log10 (p value) > 0.7. (**E**) Heatmap showing the relative abundance (log2 LFQ) of proximal proteins involved in KRAS related canonical pathways (such as MEK-RAF, mTOR, PI3K, RALGDS, RASSF and TIAM RAC pathway).

Figure 4: Interplay between KRAS and LZTR1 protein turnover, controlled by CUL3, is disrupted by KRAS mutations

(A) Heatmap showing relative abundance of known KRAS interactors in WT KRAS, G12D, G13D and Q61H KRAS mutant-APEX2 samples in either starvation or FCS stimulated condition. **(B)** APEX-2 labelling was performed in all different cell lines (WT, G12D, G13D and Q61H) under starvation and FCS induction. Western blot analysis showing ERK, pERK, ARAF and LZTR1 in cell extract as well as elution upon streptavidin-immunoprecipitation. **(C)** Cells were seeded in 96 well plates and treated with tetracycline for 24 hours. Next day cells were transfected with LZTR1 siRNA or Control siRNA. Cells were imaged after 72 hours using the Opera Phenix microscope. The images were analysed in Columbus Image Data Storage and Analysis System. The media fluorescent per well per mean per cell was determined. Finally, a fold difference between the control and the siRNA LZTR1 was measured. **(D)** Stable HEK293 FRT T-REX cell lines of WT, G12D, G13D and Q61H were treated with tetracycline for 24 hours. The next day, cells were treated with 50 µg/mL cycloheximide (CHX). At the indicated time points after CHX-treatment cells were harvested. Western blot analysis showing GFP, Pan-Ras and ACTB in cell extract was performed. **(E)** Band densities from Figure 4D were analyzed using ImageStudio, and expression was normalized to ACTB protein levels to determine KRAS half-life. **(F)** The influence of LZTR1 overexpression on WT K-Ras as well as G12D, G13D and Q61H oncogenic

mutants. HEK293 cells were seeded in 6 well plates and transfected with 1µg Flag-K-Ras plasmids as well 0, 0.1 or 0,25 µg Myc-LZTR1 plasmid concentration. Cells were cultured for a total of 48 hours before protein levels were evaluated using Western blot. **(G)** HEK293T cells were transfected with 1 µg Flag-RAS and 0.2 µg Myc-LZTR1 plasmid concentration. Cells were incubated for 48 hours, then cells were treated with 50 µg/mL CHX. At the indicated time points after CHX-treatment cells were harvested. Western blot analysis showing FLAG (RAS), MYC (LZTR1) and ACTB in cell extract was performed. **(H)** HEK293T cells were transfected with 1 µg Flag-RAS and 0.2µg Myc-LZTR1 plasmid concentration and let to grow for 48 hours. Cells were then treated for 24 hours with MLN4924 in different concentrations (0, 0.3 1 µM). Cell extract was then analysed on western blot and FLAG (RAS), MYC (LZTR1), CUL3 and ACTB was monitored. **(I)** HEK293T cells were transfected with 1 µg Flag-RAS and 0.2 µg Myc-LZTR1 plasmid concentration and let to grow for 48 hours. Cells were then treated for indicated time with MLN4924 (0.3 µM). Cell extract was then analysed on western blot and FLAG (RAS), MYC (LZTR1), CUL3 and ACTB was monitored.

Figure S1: Endogenous, APEX2-KRAS and GFP-KRAS association with membrane components

(A) Western blot indicates the biotinylated proteins in the presence or absence of different c reagents including tetracycline, phenol-biotin and H_2O_2. K-Ras APEX-2 stable cell line was treated with tetracycline for 24 hours where is indicated. Then, cells were treated with phenol-biotin and/ or H_2O_2 (where is indicated) and cells were lysed, and proteins were separated in an SDS Gel. Streptavidin, DyLight 488 Conjugated antibody were used to visualise the biotinylating proteins. * Represents biotinylated background proteins. **(B)** Western blot analysis showing a-FLAG in cell extract upon 24 hours tetracycline treatment. **(C)** Imaging of live cells using Opera Phenix™ and processed in Columbus Image Analysis System. Panels 1183 Hoechst 33342 for staining DNA (blue); the green fluorescence signal from GFP (Green), Differential Interference Contrast (DIC). **(D)** Western blot

analysis showing K-Ras GFP, GAPDH and GFP expression upon digitonin cytoplasmic-membrane fractionation of Stable K-Ras GFP or GFP only FRT T-Rex HEK293 cell line. Cells were incubated with tetracycline for 24 hours. **(E)** Western blot analysis showing a-FLAG, endogenous KRAS, TOM20 and Calreticulin expression upon digitonin cytoplasmic-membrane fractionation of stable KRAS APEX-2 WT, G12D, G13D and Q61H FRT T-Rex HEK293 cell lines. Cells were incubated with or without tetracycline for 24 hours. **(F)** Western blot analysis showing a-FLAG, GAPDH, TOM20 and endogenous KRAS in sucrose gradient fractions upon 15 hours of starvation or 15 hours of starvation and a subsequent 10-minute treatment with 20% FCS.

Figure S2: Enriched proteomes between KRAS wildtype exposed to starvation or acute FCS stimulation

(**A-B**) Volcano plotting of fold changes and p values derived from t-test statistic for proximal proteins identified in WT KRAS-APEX2 in either starvation (**A**) or FCS treated condition (**B**), in which the beads were used as a control. Known KRAS effectors (red), repressors (green) and receptors (blue) are coloured and labelled. (**C**) Histogram of proteins with differential protein abundances, reflecting enrichment per KRAS species.

Figure S3: Enriched proteomes between KRAS wildtype and G12D, G13D and Q61H mutants

(A-F) Volcano plotting of fold changes and p values derived from t-test statistic for proximal proteins identified in G12D, G13D, and Q61H KRAS mutant in either starvation or FCS treated condition, in which WT-KRAS was used as a control. Known KRAS effectors (red), repressors (green) and receptors (blue) are coloured and labelled.

Figure S4: KRAS wildtype, G12D, G13D and Q61H protein interaction networks

(**A-B**) Circos plot showing the overlap of the proximal proteins identified from three mutants in starvation (**A**) and FCS stimulation state (**B**). (**C**-**D**) Heatmap showing the top enrichment clusters with colour scale representing statistical significance, which was performed using Metascape. Gray colour indicates a lack of significance.

Figure S5: Interdependence of LZTR1 and KRAS protein stabilities controlled by CUL3

(A) Microscopy based analysis of GFP-KRAS in the presence and absence of LZTR1. (**B**) KRAS and Pan-Ras protein stability in the presence and absence of LZTR1 assessed by immunoblotting. (**C**) Cullin 3 (CUL3) knockdown stabilises LZTR1. (**D**) LZTR1 (MYC) and KRAS (FLAG) levels are correlated at the protein level. (**E**) KRAS wildtype and G12D (both FLAG tagged) differentially affect LZTR1 (MYC-tag) protein levels. (**F**) KRAS (FLAG) and LZTR1 (MYC) protein levels are dependent on the presence of Cullin 3 (CUL3).

References

Abe, T., Umeki, I., Kanno, S., Inoue, S., Niihori, T., and Aoki, Y. (2020). LZTR1 facilitates polyubiquitination and degradation of RAS-GTPases. Cell Death and Differentiation *27*, 1023-1035.

Adhikari, H., and Counter, C.M. (2018). Interrogating the protein interactomes of RAS isoforms identifies PIP5K1A as a KRAS-specific vulnerability. Nature Communications *9*.

Bigenzahn, J.W., Collie, G.M., Kartnig, F., Pieraks, M., Vladimer, G.I., Heinez, L.X., Sedlyarov, V., Schischlik, F., Fauster, A., Rebsamen, M.*, et al.* (2018). LZTR1 is a regulator of RAS ubiquitination and signaling. Science *362*, 1171-+.

Buday, L., and Downward, J. (1993). Epidermal Growth-Factor Regulates P21(Ras) through the Formation of a Complex of Receptor, Grb2 Adapter Protein, and Sos Nucleotide Exchange Factor. Cell *73*, 611-620.

Castellano, E., and Downward, J. (2010). Role of RAS in the regulation of PI 3-kinase. Curr Top Microbiol Immunol *346*, 143-169.

Cheng, D.K., Oni, T.E., Thalappillil, J.S., Park, Y., Ting, H.C., Alagesan, B., Prasad, N.V., Addison, K., Rivera, K.D., Pappin, D.J.*, et al.* (2021). Oncogenic KRAS engages an RSK1/NF1 pathway to inhibit wild-type RAS signaling in pancreatic cancer. Proc Natl Acad Sci U S A *118*.

Choi, H., Liu, G., Mellacheruvu, D., Tyers, M., Gingras, A.C., and Nesvizhskii, A.I. (2012). Analyzing protein-protein interactions from affinity purification-mass spectrometry data with SAINT. Curr Protoc Bioinformatics *Chapter 8*, Unit8 15.

Cook, J.H., Melloni, G.E.M., Gulhan, D.C., Park, P.J., and Haigis, K.M. (2021). The origins and genetic interactions of KRAS mutations are allele- and tissue-specific. Nat Commun *12*, 1808.

Fischer, R., and Kessler, B.M. (2015). Gel-aided sample preparation (GASP)--a simplified method for gel-assisted proteomic sample generation from protein extracts and intact cells. Proteomics *15*, 1224-1229.

Geiger, T., Wehner, A., Schaab, C., Cox, J., and Mann, M. (2012). Comparative proteomic analysis of eleven common cell lines reveals ubiquitous but varying expression of most proteins. Mol Cell Proteomics *11*, M111 014050.

Gimple, R.C., and Wang, X.X. (2019). RAS: Striking at the Core of the Oncogenic Circuitry. Frontiers in Oncology *9*.

Giurgiu, M., Reinhard, J., Brauner, B., Dunger-Kaltenbach, I., Fobo, G., Frishman, G., Montrone, C., and Ruepp, A. (2019). CORUM: the comprehensive resource of mammalian protein complexes-2019. Nucleic Acids Res *47*, D559-D563.

Haigis, K.M. (2017). KRAS Alleles: The Devil Is in the Detail. Trends in Cancer *3*, 686-697.

Hollstein, P.E., and Cichowski, K. (2013). Identifying the Ubiquitin Ligase Complex that Regulates the NF1 Tumor Suppressor and Ras. Cancer Discov *3*, 880-893.

Ito, R.E., Oneyama, C., and Aoki, K. (2021). Oncogenic mutation or overexpression of oncogenic KRAS or BRAF is not sufficient to confer oncogene addiction. PLoS One *16*, e0249388.

Kiel, C., Matallanas, D., and Kolch, W. (2021). The Ins and Outs of RAS Effector Complexes. Biomolecules *11*.

Killoran, R.C., and Smith, M.J. (2019). Conformational resolution of nucleotide cycling and effector interactions for multiple small GTPases determined in parallel. J Biol Chem *294*, 9937-9948.

Kovalski, J.R., Bhaduri, A., Zehnder, A.M., Neela, P.H., Che, Y., Wozniak, G.G., and Khavari, P.A. (2019). The Functional Proximal Proteome of Oncogenic Ras Includes mTORC2. Mol Cell *73*, 830-844 e812.

Kunimasa, K., Hirotsu, Y., Nakamura, H., Tamiya, M., Iijima, Y., Ishida, H., Hamamoto, Y., Maniwa, T., Kimura, T., Nishino, K.*, et al.* (2020). Rapid progressive lung cancers harbouring multiple clonal driver mutations with big bang evolution model. Cancer Genet *241*, 51-56.

Lambert, J.M., Lambert, Q.T., Reuther, G.W., Malliri, A., Siderovski, D.P., Sondek, J., Collard, J.G., and Der, C.J. (2002). Tiam1 mediates Ras activation of Rac by a PI(3)K-independent mechanism. Nature Cell Biology *4*, 621-625.

Li, X., Cheng, Z., and Jin, H. (2012). Dynamics of Ras complexes observed in living cells. Sensors (Basel) *12*, 9411-9422.

Liu, P., Wang, Y., and Li, X. (2019). Targeting the untargetable KRAS in cancer therapy. Acta Pharm Sin B *9*, 871-879.

Matallanas, D., Arozarena, I., Berciano, M.T., Aaronson, D.S., Pellicer, A., Lafarga, M., and Crespo, P. (2003). Differences on the inhibitory specificities of H-Ras, K-Ras, and N-Ras (N17) dominant negative mutants are related to their membrane microlocalization. J Biol Chem *278*, 4572-4581.

Milhollen, M.A., Traore, T., Adams-Duffy, J., Thomas, M.P., Berger, A.J., Dang, L., Dick, L.R., Garnsey, J.J., Koenig, E., Langston, S.P.*, et al.* (2010). MLN4924, a NEDD8-activating enzyme inhibitor, is active in diffuse large B-cell lymphoma models: rationale for treatment of NF-kappa B-dependent lymphoma. Blood *116*, 1515-1523.

Moodie, S.A., Willumsen, B.M., Weber, M.J., and Wolfman, A. (1993). Complexes of Ras.Gtp with Raf-1 and Mitogen-Activated Protein-Kinase Kinase. Science *260*, 1658-1661.

Motta, M., Fidan, M., Bellacchio, E., Pantaleoni, F., Schneider-Heieck, K., Coppola, S., Borck, G., Salviati, L., Zenker, M., Cirstea, I.C.*, et al.* (2019). Dominant Noonan syndrome-causing LZTR1

mutations specifically affect the Kelch domain substrate-recognition surface and enhance RAS-MAPK signaling. Hum Mol Genet *28*, 1007-1022.

Pintacuda, G., Lassen, F.H., Hsu, Y.H.H., Kim, A., Martin, J.M., Malolepsza, E., Lim, J.K., Fornelos, N., Eggan, K.C., and Lage, K. (2021). Genoppi is an open-source software for robust and standardized integration of proteomic and genetic data. Nature Communications *12*.

Prior, I.A., Lewis, P.D., and Mattos, C. (2012). A comprehensive survey of Ras mutations in cancer. Cancer Res *72*, 2457-2467.

Rabara, D., Tran, T.H., Dharmaiah, S., Stephens, R.M., McCormick, F., Simanshu, D.K., and Holderfield, M. (2019). KRAS G13D sensitivity to neurofibromin-mediated GTP hydrolysis. Proceedings of the National Academy of Sciences of the United States of America *116*, 22122-22131.

Semenas, J., Hedblom, A., Miftakhova, R.R., Sarwar, M., Larsson, R., Shcherbina, L., Johansson, M.E., Harkonen, P., Sterner, O., and Persson, J.L. (2014). The role of PI3K/AKT-related PIP5K1alpha and the discovery of its selective inhibitor for treatment of advanced prostate cancer. Proc Natl Acad Sci U S A *111*, E3689-3698.

Steklov, M., Pandolf, S., Baietti, M.F., Batiuk, A., Carai, P., Najm, P., Zhang, M., Jang, H., Renzi, F., Cai, Y.*, et al.* (2018). Mutations in LZTR1 drive human disease by dysregulating RAS ubiquitination. Science *362*, 1177-+.

Taieb, J., Le Malicot, K., Shi, Q., Penault-Llorca, F., Bouche, O., Tabernero, J., Mini, E., Goldberg, R.M., Folprecht, G., Luc Van Laethem, J.*, et al.* (2017). Prognostic Value of BRAF and KRAS Mutations in MSI and MSS Stage III Colon Cancer. J Natl Cancer Inst *109*.

Teo, G.C., Liu, G.M., Zhang, J.P., Nesvizhskii, A.I., Gingras, A.C., and Choi, H. (2014). SAINTexpress: Improvements and additional features in Significance Analysis of INTeractome software. Journal of Proteomics *100*, 37-43.

Trinkle-Mulcahy, L. (2019). Recent advances in proximity-based labeling methods for interactome mapping. F1000Res *8*.

Vigil, D., Cherfils, J., Rossman, K.L., and Der, C.J. (2010). Ras superfamily GEFs and GAPs: validated and tractable targets for cancer therapy? Nature Reviews Cancer *10*, 842-857.

Wong, C.H., Li, Y.J., and Chen, Y.C. (2016). Therapeutic potential of targeting acinar cell reprogramming in pancreatic cancer. World J Gastroenterol *22*, 7046-7057.

Yin, G.W., Zhang, J., Nair, V., Truong, V., Chaia, A., Petela, J., Harrison, J., Gorfe, A.A., and Campbell, S.L. (2020). KRAS Ubiquitination at Lysine 104 Retains Exchange Factor Regulation by Dynamically Modulating the Conformation of the Interface. Iscience *23*.

Zhou, Y., Zhou, B., Pache, L., Chang, M., Khodabakhshi, A.H., Tanaseichuk, O., Benner, C., and Chanda, S.K. (2019). Metascape provides a biologist-oriented resource for the analysis of systems-level datasets. Nat Commun *10*, 1523.

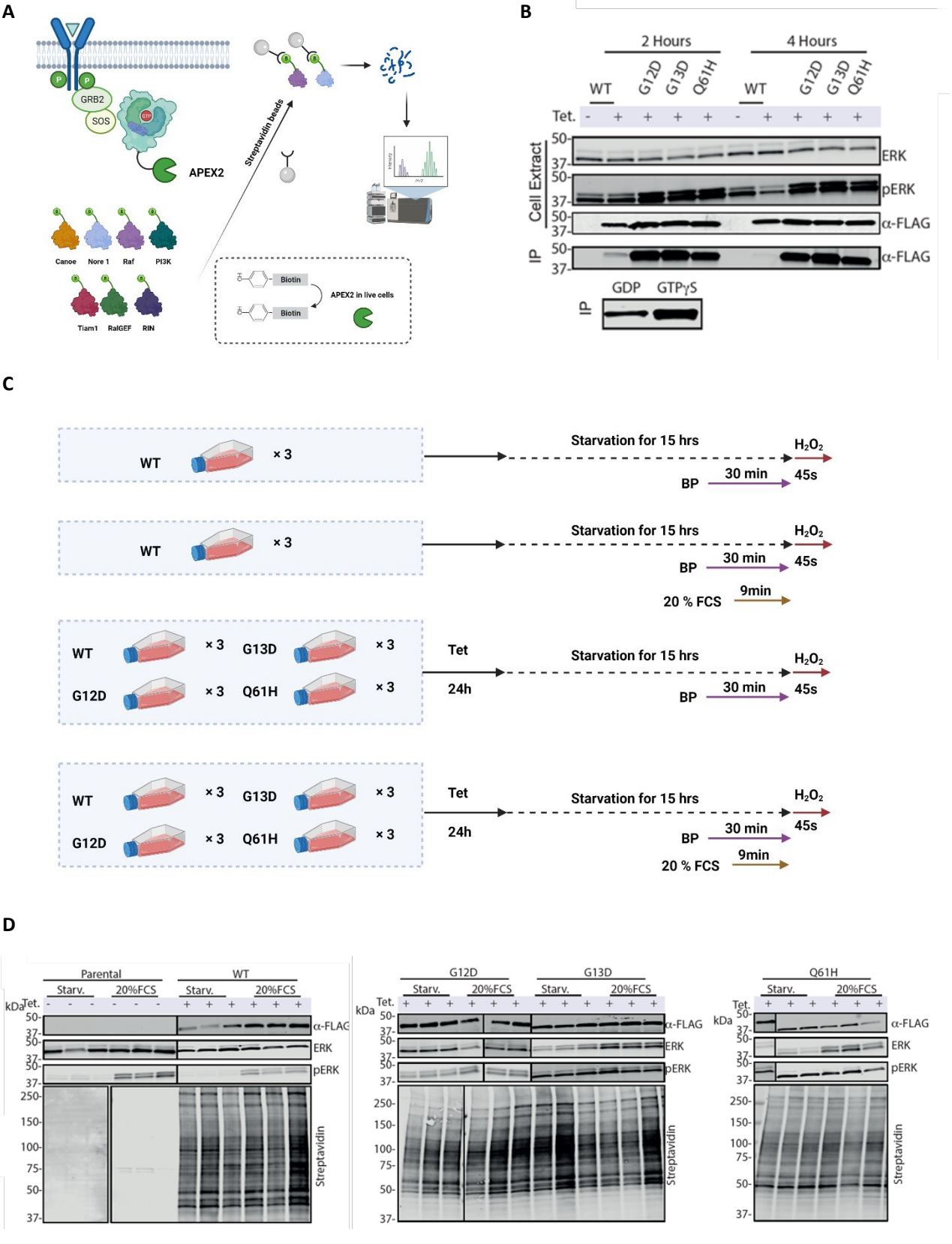
A
GRB2
SOS
APEX2
Streptavidin beads
Canoe
Nore 1
Raf
PI3K
Tiam1
RalGEF
RIN
Biotin
Biotin
APEX2 in live cells
B
2 Hours
4 Hours
WT
G12D
G13D
Q61H
WT
G12D
G13D
Q61H
Tet.
Cell Extract
ERK
pERK
α-FLAG
IP
α-FLAG
GDP
GTPγS
IP
C
WT
× 3
Starvation for 15 hrs
H2O2
BP
30 min
45s
WT
× 3
Starvation for 15 hrs
H2O2
BP
30 min
45s
20 % FCS
9min
WT
× 3
G13D
× 3
G12D
× 3
Q61H
× 3
Tet
24h
Starvation for 15 hrs
H2O2
BP
30 min
45s
WT
× 3
G13D
× 3
G12D
× 3
Q61H
× 3
Tet
24h
Starvation for 15 hrs
H2O2
BP
30 min
45s
20 % FCS
9min
D
Parental
WT
Starv.
20%FCS
Starv.
20%FCS
Tet.
kDa
α-FLAG
ERK
pERK
Streptavidin
G12D
G13D
Q61H
Starv.
20%FCS
Tet.
kDa
α-FLAG
ERK
pERK
Streptavidin

Figure 2

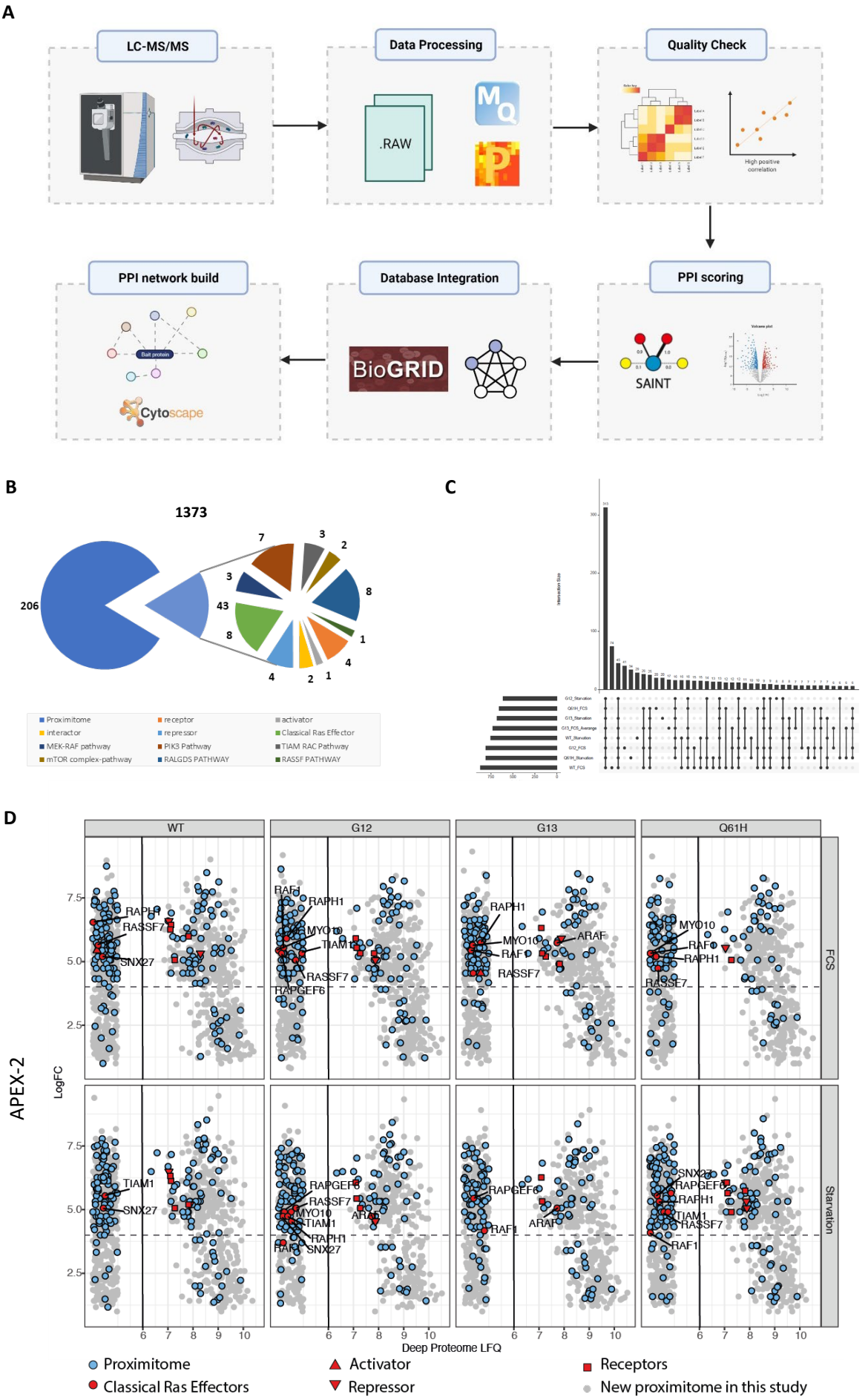
A
LC-MS/MS
Data Processing
.RAW
Quality Check
High positive correlation
PPI scoring
SAINT
Database Integration
BioGRID
PPI network build
Bait protein
Cytoscape
B
1373
206
43
Proximitome
receptor
activator
interactor
repressor
Classical Ras Effector
MEK-RAF pathway
PIK3 Pathway
TIAM RAC Pathway
mTOR complex-pathway
RALGDS PATHWAY
RASSF PATHWAY
C
D
APEX-2
WT
G12
G13
Q61H
FCS
Starvation
LogFC
Deep Proteome LFQ
RAPH1
RASSF7
SNX27
MYO10
TIAM1
RAPGEF6
RAF1
ARAF
Proximitome
Classical Ras Effectors
Activator
Repressor
Receptors
New proximitome in this study

Figure 3 Comparison between WT and MT

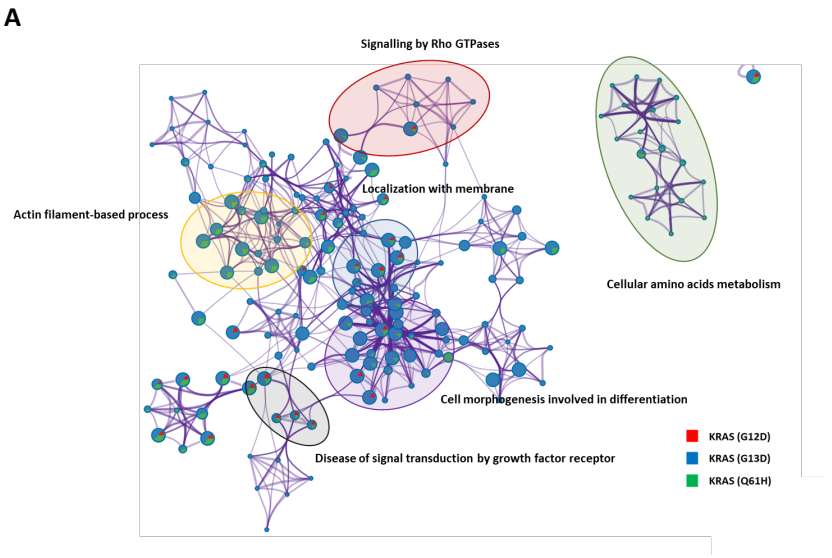

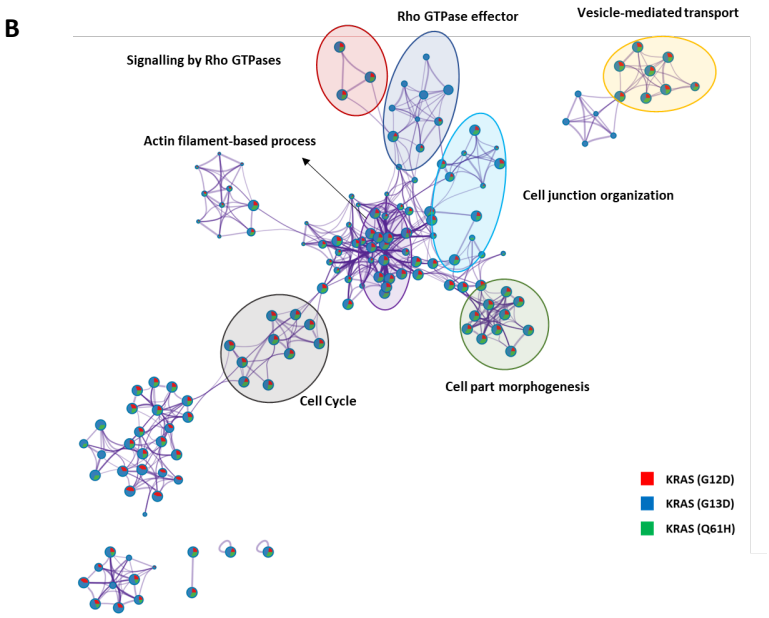

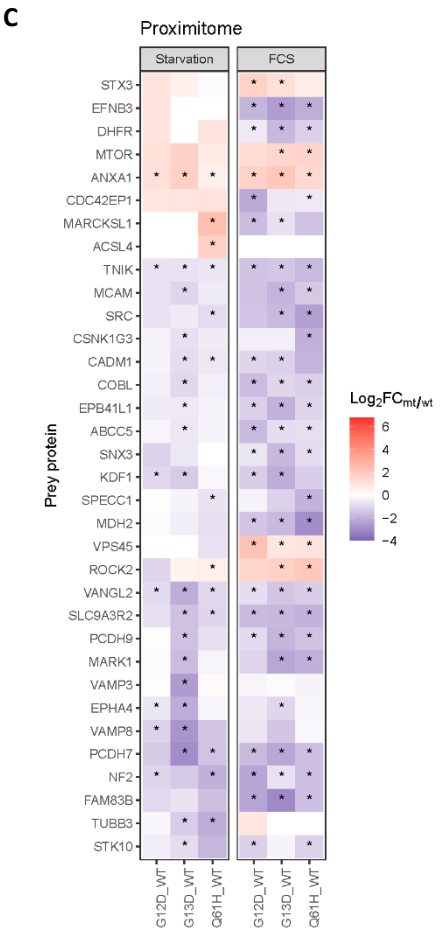

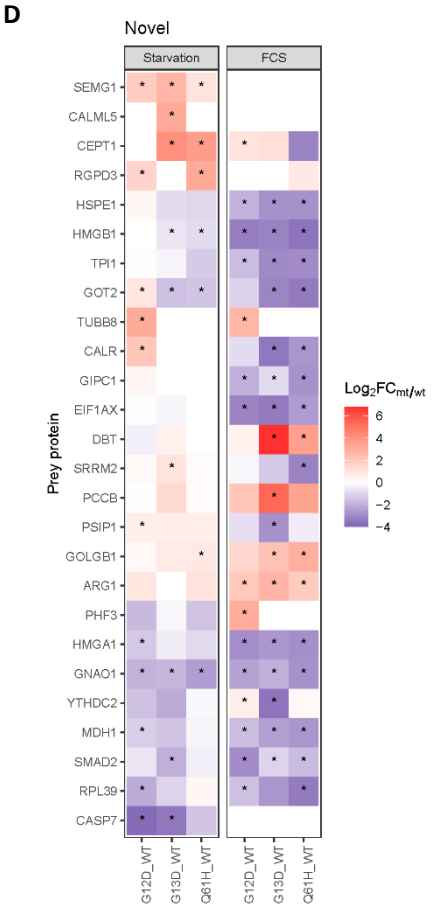

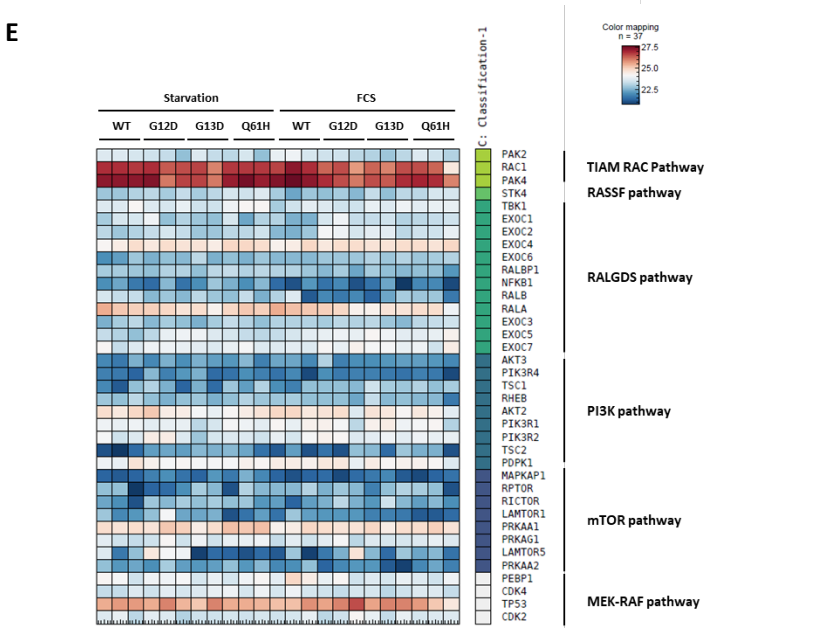

Figure 4

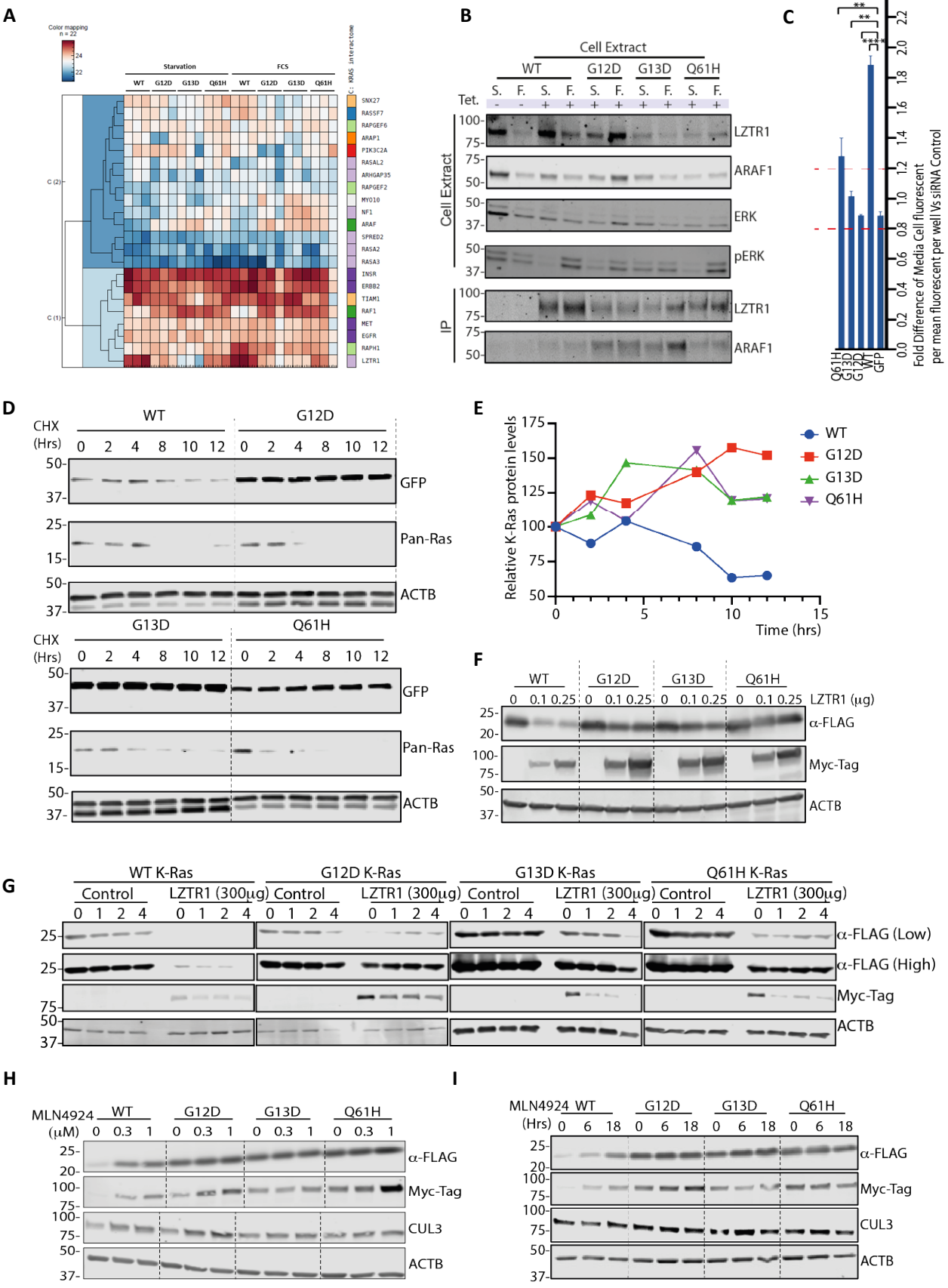
A
Color mapping n = 22
Starvation
FCS
WT G12D G13D Q61H WT G12D G13D Q61H
C: KRAS interactome
SNX27
RASSF7
RAPGEF6
ARAP1
PIK3C2A
RASAL2
ARHGAP35
RAPGEF2
MYO10
NF1
ARAF
SPRED2
RASA2
RASA3
INSR
ERBB2
TIAM1
RAF1
MET
EGFR
RAPH1
LZTR1
C (2)
C (1)
B
Cell Extract
WT G12D G13D Q61H
Tet.
S. F. S. F. S. F. S. F. S. F.
Cell Extract
IP
LZTR1
ARAF1
ERK
pERK
C
Fold Difference of Media Cell fluorescent per mean fluorescent per well Vs siRNA Control
Q61H
G13D
G12D
WT
GFP
D
CHX (Hrs)
WT
G12D
G13D
Q61H
0 2 4 8 10 12
GFP
Pan-Ras
ACTB
E
Relative K-Ras protein levels
Time (hrs)
WT
G12D
G13D
Q61H
F
WT G12D G13D Q61H
0 0.1 0.25
LZTR1 (µg)
α-FLAG
Myc-Tag
ACTB
G
WT K-Ras
G12D K-Ras
G13D K-Ras
Q61H K-Ras
Control
LZTR1 (300µg)
0 1 2 4
α-FLAG (Low)
α-FLAG (High)
Myc-Tag
ACTB
H
MLN4924 (µM)
WT G12D G13D Q61H
0 0.3 1
α-FLAG
Myc-Tag
CUL3
ACTB
I
MLN4924 (Hrs)
WT G12D G13D Q61H
0 6 18
α-FLAG
Myc-Tag
CUL3
ACTB
J
KRASWT
LZTR1
Cullin-3
T1/2
KRASMut
LZTR1
Cullin-3

Figure S1

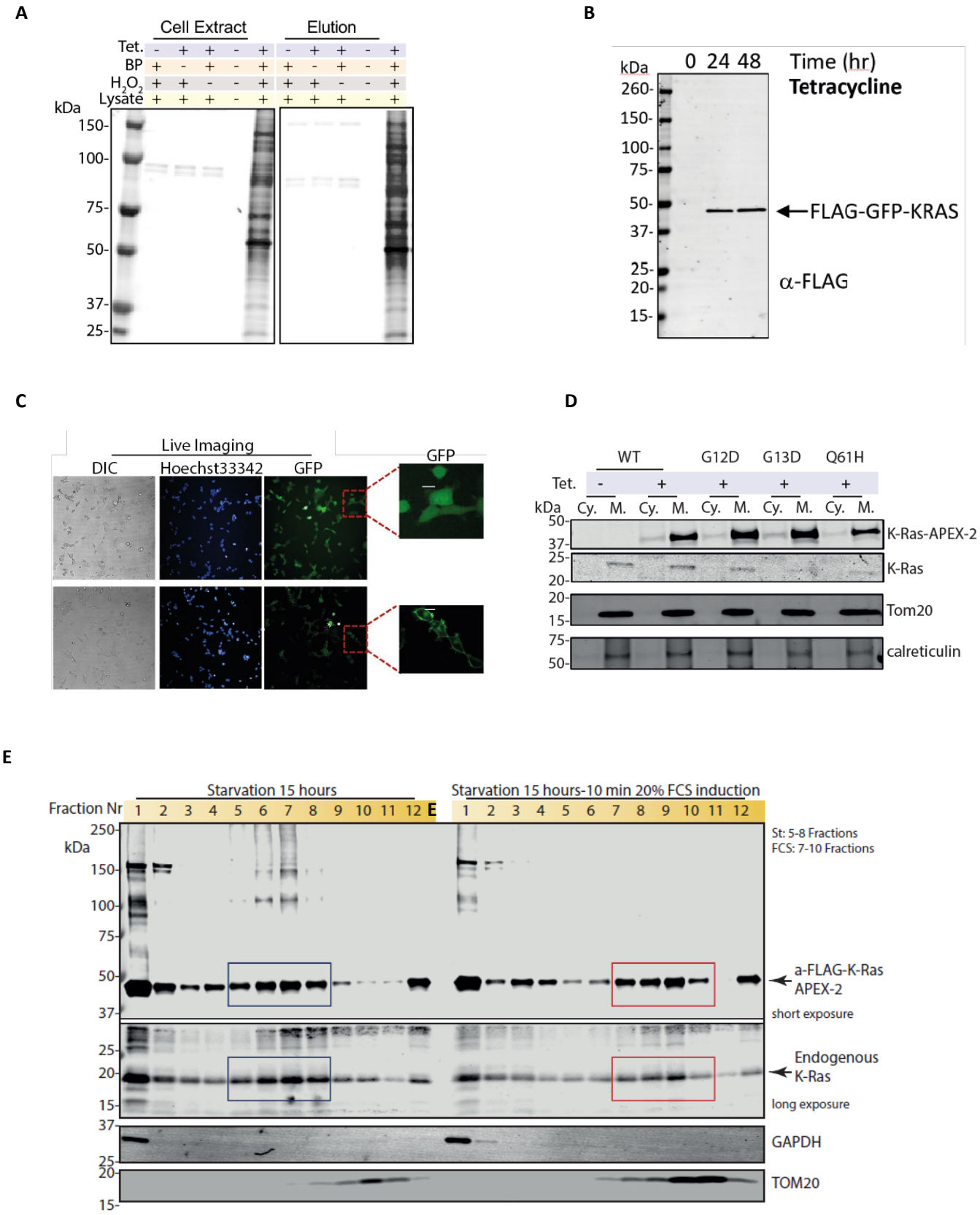
A
Cell Extract
Elution
Tet.
BP
H_2O_2
Lysate
kDa
150-
100-
75-
50-
37-
25-
B
kDa
0 24 48
Time (hr)
Tetracycline
260-
150-
100-
75-
50-
37-
25-
20-
15-
FLAG-GFP-KRAS
α-FLAG
C
Live Imaging
DIC
Hoechst33342
GFP
GFP
D
WT
G12D
G13D
Q61H
Tet.
kDa
Cy.
M.
K-Ras-APEX-2
K-Ras
Tom20
calreticulin
E
Starvation 15 hours
Starvation 15 hours-10 min 20% FCS induction
Fraction Nr
St: 5-8 Fractions
FCS: 7-10 Fractions
a-FLAG-K-Ras APEX-2
short exposure
Endogenous K-Ras
long exposure
GAPDH
TOM20

Figure S2

A

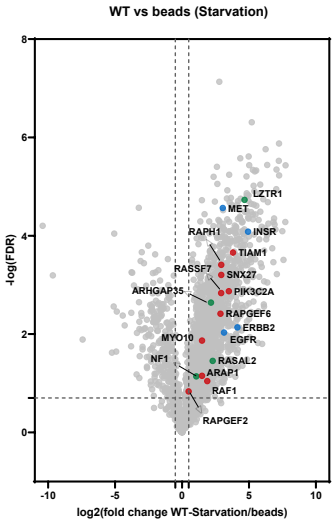

B

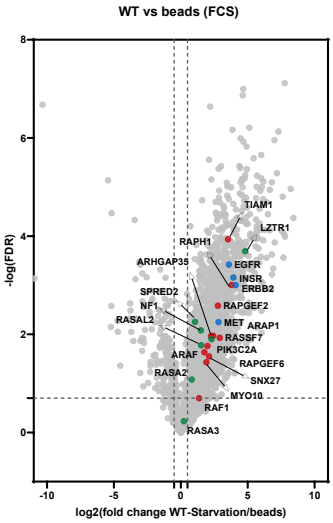

C

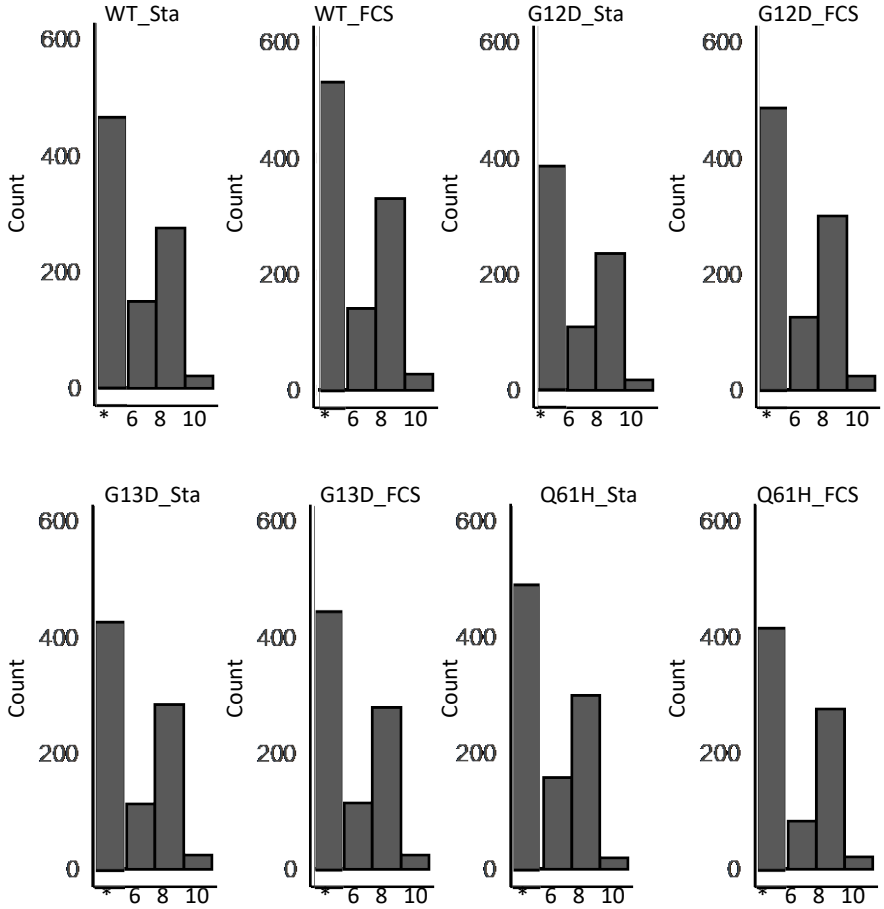

Figure S3

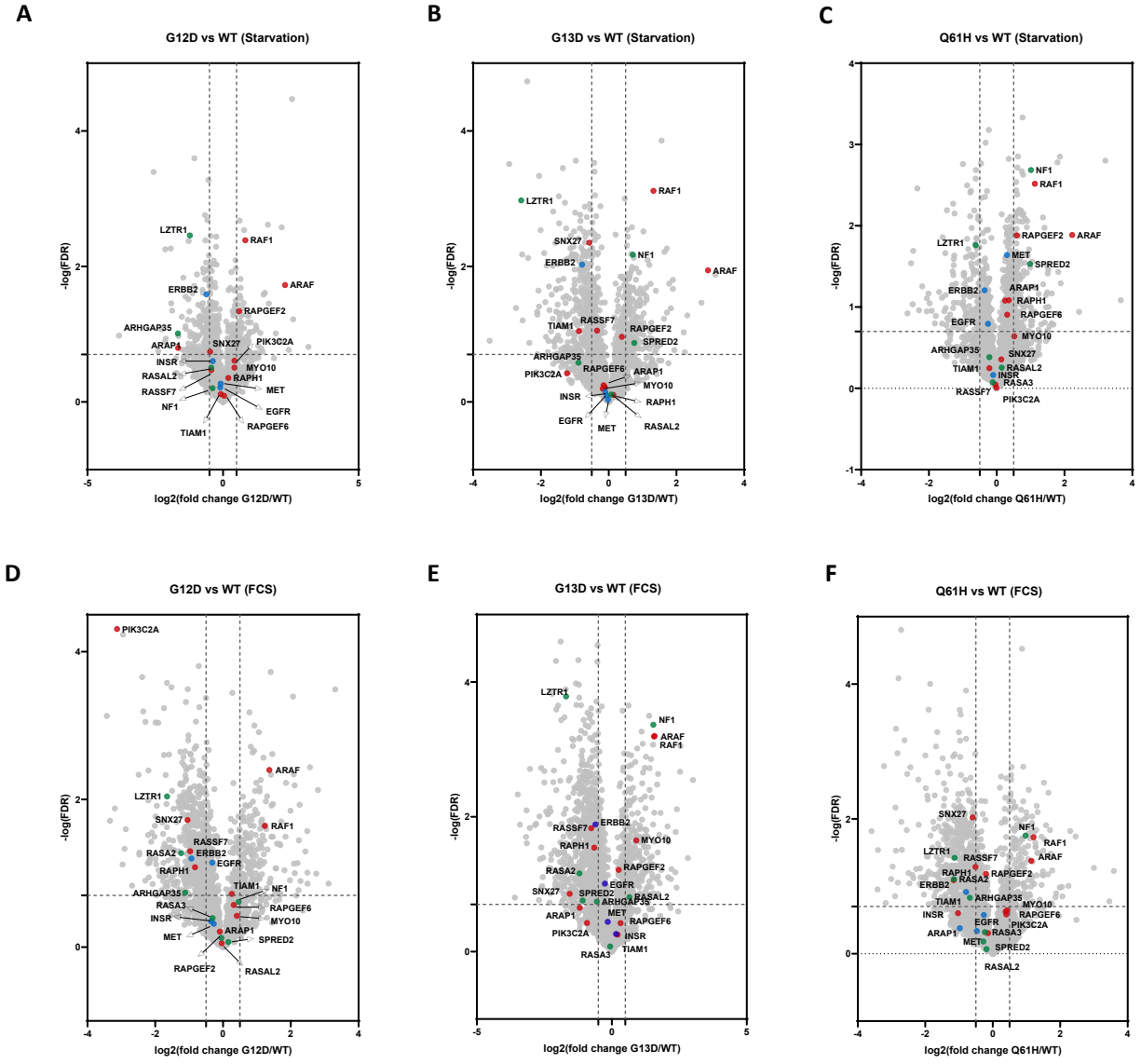
A
G12D vs WT (Starvation)
-log(FDR)
log2(fold change G12D/WT)
LZTR1
RAF1
ARAF
ERBB2
RAPGEF2
ARHGAP35
ARAP1
SNX27
PIK3C2A
INSR
MYO10
RASAL2
RAPH1
RASSF7
MET
NF1
EGFR
TIAM1
RAPGEF6
B
G13D vs WT (Starvation)
-log(FDR)
log2(fold change G13D/WT)
RAF1
LZTR1
SNX27
NF1
ERBB2
ARAF
TIAM1
RASSF7
RAPGEF2
SPRED2
ARHGAP35
RAPGEF6
ARAP1
PIK3C2A
MYO10
INSR
RAPH1
EGFR
MET
RASAL2
C
Q61H vs WT (Starvation)
-log(FDR)
log2(fold change Q61H/WT)
NF1
RAF1
RAPGEF2
ARAF
LZTR1
MET
SPRED2
ERBB2
ARAP1
RAPH1
RAPGEF6
EGFR
MYO10
ARHGAP35
SNX27
TIAM1
RASAL2
INSR
RASA3
RASSF7
PIK3C2A
D
G12D vs WT (FCS)
-log(FDR)
log2(fold change G12D/WT)
PIK3C2A
ARAF
LZTR1
SNX27
RAF1
RASSF7
RASA2
ERBB2
EGFR
RAPH1
TIAM1
NF1
ARHGAP35
RASA3
RAPGEF6
INSR
MYO10
ARAP1
MET
SPRED2
RAPGEF2
RASAL2
E
G13D vs WT (FCS)
-log(FDR)
log2(fold change G13D/WT)
LZTR1
NF1
ARAF
RAF1
RASSF7
ERBB2
MYO10
RAPH1
RAPGEF2
RASA2
EGFR
SNX27
SPRED2
RASAL2
ARHGAP35
ARAP1
MET
RAPGEF6
PIK3C2A
INSR
RASA3
TIAM1
F
Q61H vs WT (FCS)
-log(FDR)
log2(fold change Q61H/WT)
SNX27
NF1
RAF1
LZTR1
RASSF7
ARAF
RAPH1
RAPGEF2
RASA2
ERBB2
TIAM1
ARHGAP35
MYO10
INSR
RAPGEF6
EGFR
PIK3C2A
ARAP1
RASA3
MET
SPRED2
RASAL2

Figure S4

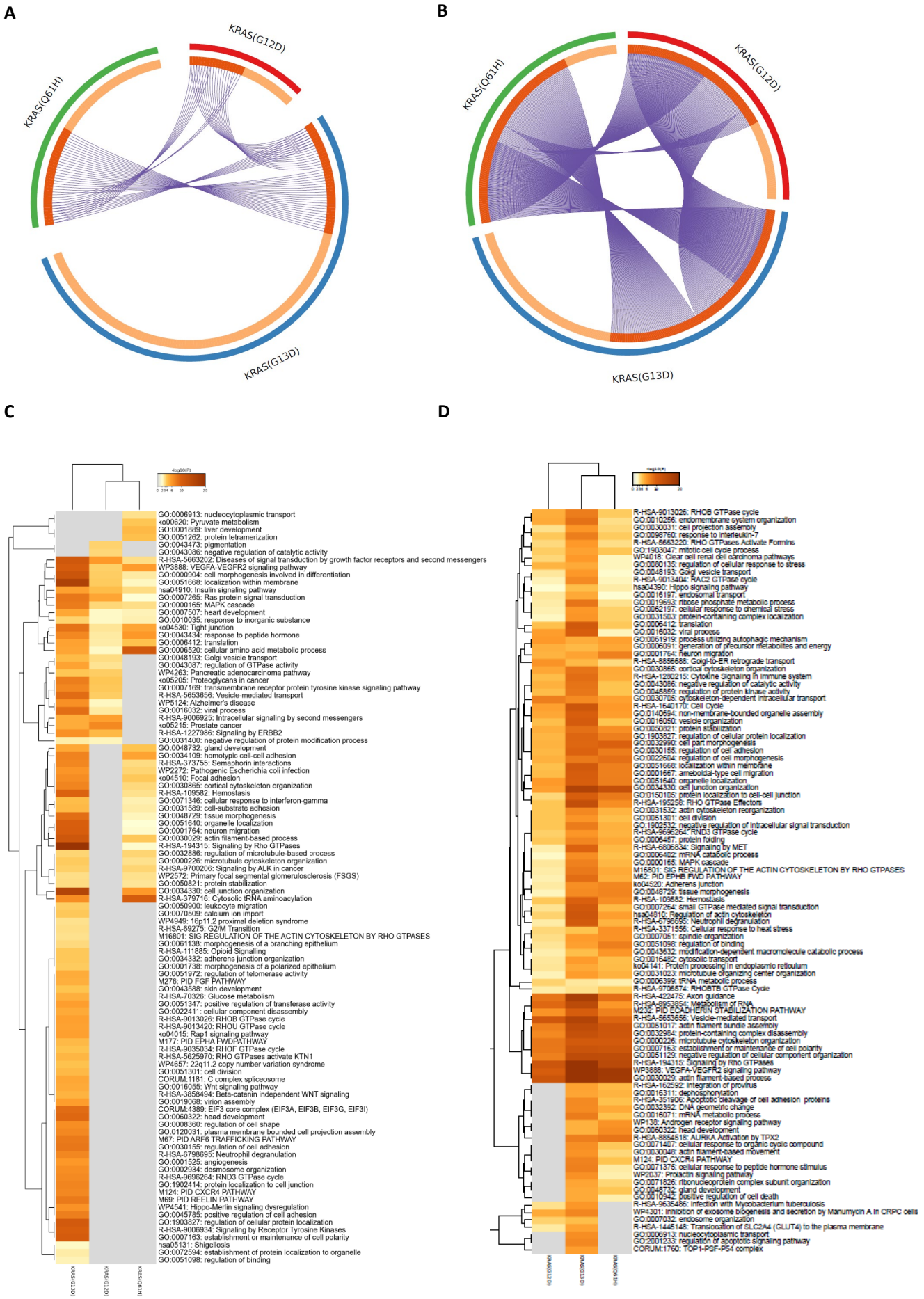
A
KRAS(G12D)
KRAS(Q61H)
KRAS(G13D)
B
KRAS(Q61H)
KRAS(G12D)
KRAS(G13D)
C
-log10(P)
GO:0006913: nucleocytoplasmic transport
ko00620: Pyruvate metabolism
GO:0001889: liver development
GO:0051262: protein tetramerization
GO:0043473: pigmentation
GO:0043086: negative regulation of catalytic activity
R-HSA-5663202: Diseases of signal transduction by growth factor receptors and second messengers
WP3888: VEGFA-VEGFR2 signaling pathway
GO:0000904: cell morphogenesis involved in differentiation
GO:0051668: localization within membrane
hsa04910: Insulin signaling pathway
GO:0007265: Ras protein signal transduction
GO:0000165: MAPK cascade
GO:0007507: heart development
GO:0010035: response to inorganic substance
ko04530: Tight junction
GO:0043434: response to peptide hormone
GO:0006412: translation
GO:0006520: cellular amino acid metabolic process
GO:0048193: Golgi vesicle transport
GO:0043087: regulation of GTPase activity
WP4263: Pancreatic adenocarcinoma pathway
ko05205: Proteoglycans in cancer
GO:0007169: transmembrane receptor protein tyrosine kinase signaling pathway
R-HSA-5653656: Vesicle-mediated transport
WP5124: Alzheimer's disease
GO:0016032: viral process
R-HSA-9006925: Intracellular signaling by second messengers
ko05215: Prostate cancer
R-HSA-1227986: Signaling by ERBB2
GO:0031400: negative regulation of protein modification process
GO:0048732: gland development
GO:0034109: homotypic cell-cell adhesion
R-HSA-373755: Semaphorin interactions
WP2272: Pathogenic Escherichia coli infection
ko04510: Focal adhesion
GO:0030865: cortical cytoskeleton organization
R-HSA-109582: Hemostasis
GO:0071346: cellular response to interferon-gamma
GO:0031589: cell-substrate adhesion
GO:0048729: tissue morphogenesis
GO:0051640: organelle localization
GO:0001764: neuron migration
GO:0030029: actin filament-based process
R-HSA-194315: Signaling by Rho GTPases
GO:0032886: regulation of microtubule-based process
GO:0000226: microtubule cytoskeleton organization
R-HSA-9700206: Signaling by ALK in cancer
WP2572: Primary focal segmental glomerulosclerosis (FSGS)
GO:0050821: protein stabilization
GO:0034330: cell junction organization
R-HSA-379716: Cytosolic tRNA aminoacylation
GO:0050900: leukocyte migration
GO:0070509: calcium ion import
WP4949: 16p11.2 proximal deletion syndrome
R-HSA-69275: G2/M Transition
M16801: SIG REGULATION OF THE ACTIN CYTOSKELETON BY RHO GTPASES
GO:0061138: morphogenesis of a branching epithelium
R-HSA-111885: Opioid Signalling
GO:0034332: adherens junction organization
GO:0001738: morphogenesis of a polarized epithelium
GO:0051972: regulation of telomerase activity
M276: PID FGF PATHWAY
GO:0043588: skin development
R-HSA-70326: Glucose metabolism
GO:0051347: positive regulation of transferase activity
GO:0022411: cellular component disassembly
R-HSA-9013026: RHOB GTPase cycle
R-HSA-9013420: RHOU GTPase cycle
ko04015: Rap1 signaling pathway
M177: PID EPHA FWDPATHWAY
R-HSA-9035034: RHOF GTPase cycle
R-HSA-5625970: RHO GTPases activate KTN1
WP4657: 22q11.2 copy number variation syndrome
GO:0051301: cell division
CORUM:1181: C complex spliceosome
GO:0016055: Wnt signaling pathway
R-HSA-3858494: Beta-catenin independent WNT signaling
GO:0019068: virion assembly
CORUM:4389: EIF3 core complex (EIF3A, EIF3B, EIF3G, EIF3I)
GO:0060322: head development
GO:0008360: regulation of cell shape
GO:0120031: plasma membrane bounded cell projection assembly
M67: PID ARF6 TRAFFICKING PATHWAY
GO:0030155: regulation of cell adhesion
R-HSA-6798695: Neutrophil degranulation
GO:0001525: angiogenesis
GO:0002934: desmosome organization
R-HSA-9696264: RND3 GTPase cycle
GO:1902414: protein localization to cell junction
M124: PID CXCR4 PATHWAY
M69: PID REELIN PATHWAY
WP4541: Hippo-Merlin signaling dysregulation
GO:0045785: positive regulation of cell adhesion
GO:1903827: regulation of cellular protein localization
R-HSA-9006934: Signaling by Receptor Tyrosine Kinases
GO:0007163: establishment or maintenance of cell polarity
hsa05131: Shigellosis
GO:0072594: establishment of protein localization to organelle
GO:0051098: regulation of binding
KRAS(G13D)
KRAS(G12D)
KRAS(Q61H)
D
-log10(P)
R-HSA-9013026: RHOB GTPase cycle
GO:0010256: endomembrane system organization
GO:0030031: cell projection assembly
GO:0096760: response to interleukin-7
R-HSA-5663220: RHO GTPases Activate Formins
GO:1903047: mitotic cell cycle process
WP4018: Clear cell renal cell carcinoma pathways
GO:0080135: regulation of cellular response to stress
GO:0048193: Golgi vesicle transport
R-HSA-9013404: RAC2 GTPase cycle
hsa04390: Hippo signaling pathway
GO:0016197: endosomal transport
GO:0019693: ribose phosphate metabolic process
GO:0062197: cellular response to chemical stress
GO:0031503: protein-containing complex localization
GO:0006412: translation
GO:0016032: viral process
GO:0061919: process utilizing autophagic mechanism
GO:0006091: generation of precursor metabolites and energy
GO:0001764: neuron migration
R-HSA-8856688: Golgi-to-ER retrograde transport
GO:0030865: cortical cytoskeleton organization
R-HSA-1280215: Cytokine Signaling in Immune system
GO:0043086: negative regulation of catalytic activity
GO:0045859: regulation of protein kinase activity
GO:0030705: cytoskeleton-dependent intracellular transport
R-HSA-1640170: Cell Cycle
GO:0140694: non-membrane-bounded organelle assembly
GO:0016050: vesicle organization
GO:0050821: protein stabilization
GO:1903827: regulation of cellular protein localization
GO:0032990: cell part morphogenesis
GO:0030155: regulation of cell adhesion
GO:0022604: regulation of cell morphogenesis
GO:0051668: localization within membrane
GO:0001667: ameboidal-type cell migration
GO:0051640: organelle localization
GO:0034330: cell junction organization
GO:0150105: protein localization to cell-cell junction
R-HSA-195258: RHO GTPase Effectors
GO:0031532: actin cytoskeleton reorganization
GO:0051301: cell division
GO:1902532: negative regulation of intracellular signal transduction
R-HSA-9696264: RND3 GTPase cycle
GO:0006457: protein folding
R-HSA-6806834: Signaling by MET
GO:0006402: mRNA catabolic process
GO:0000165: MAPK cascade
M16801: SIG REGULATION OF THE ACTIN CYTOSKELETON BY RHO GTPASES
M62: PID EPHB FWD PATHWAY
ko04520: Adherens junction
GO:0048729: tissue morphogenesis
R-HSA-109582: Hemostasis
GO:0007264: small GTPase mediated signal transduction
hsa04810: Regulation of actin cytoskeleton
R-HSA-6798695: Neutrophil degranulation
R-HSA-3371556: Cellular response to heat stress
GO:0007051: spindle organization
GO:0051098: regulation of binding
GO:0043632: modification-dependent macromolecule catabolic process
GO:0016482: cytosolic transport
ko04141: Protein processing in endoplasmic reticulum
GO:0031023: microtubule organizing center organization
GO:0006399: tRNA metabolic process
R-HSA-9706574: RHOBTB GTPase Cycle
R-HSA-422475: Axon guidance
R-HSA-8953854: Metabolism of RNA
M232: PID ECADHERIN STABILIZATION PATHWAY
R-HSA-5653656: Vesicle-mediated transport
GO:0051017: actin filament bundle assembly
GO:0032984: protein-containing complex disassembly
GO:0000226: microtubule cytoskeleton organization
GO:0007163: establishment or maintenance of cell polarity
GO:0051129: negative regulation of cellular component organization
R-HSA-194315: Signaling by Rho GTPases
WP3888: VEGFA-VEGFR2 signaling pathway
GO:0030029: actin filament-based process
R-HSA-162592: Integration of provirus
GO:0016311: dephosphorylation
R-HSA-351906: Apoptotic cleavage of cell adhesion proteins
GO:0032392: DNA geometric change
GO:0016071: mRNA metabolic process
WP138: Androgen receptor signaling pathway
GO:0060322: head development
R-HSA-8854518: AURKA Activation by TPX2
GO:0071407: cellular response to organic cyclic compound
GO:0030048: actin filament-based movement
M124: PID CXCR4 PATHWAY
GO:0071375: cellular response to peptide hormone stimulus
WP2037: Prolactin signaling pathway
GO:0071826: ribonucleoprotein complex subunit organization
GO:0048732: gland development
GO:0010942: positive regulation of cell death
R-HSA-9635486: Infection with Mycobacterium tuberculosis
WP4301: Inhibition of exosome biogenesis and secretion by Manumycin A in CRPC cells
GO:0007032: endosome organization
R-HSA-1445148: Translocation of SLC2A4 (GLUT4) to the plasma membrane
GO:0006913: nucleocytoplasmic transport
GO:2001233: regulation of apoptotic signaling pathway
CORUM:1760: TOP1-PSF-PS4 complex
KRAS(G13D)
KRAS(G12D)
KRAS(Q61H)

Figure S5

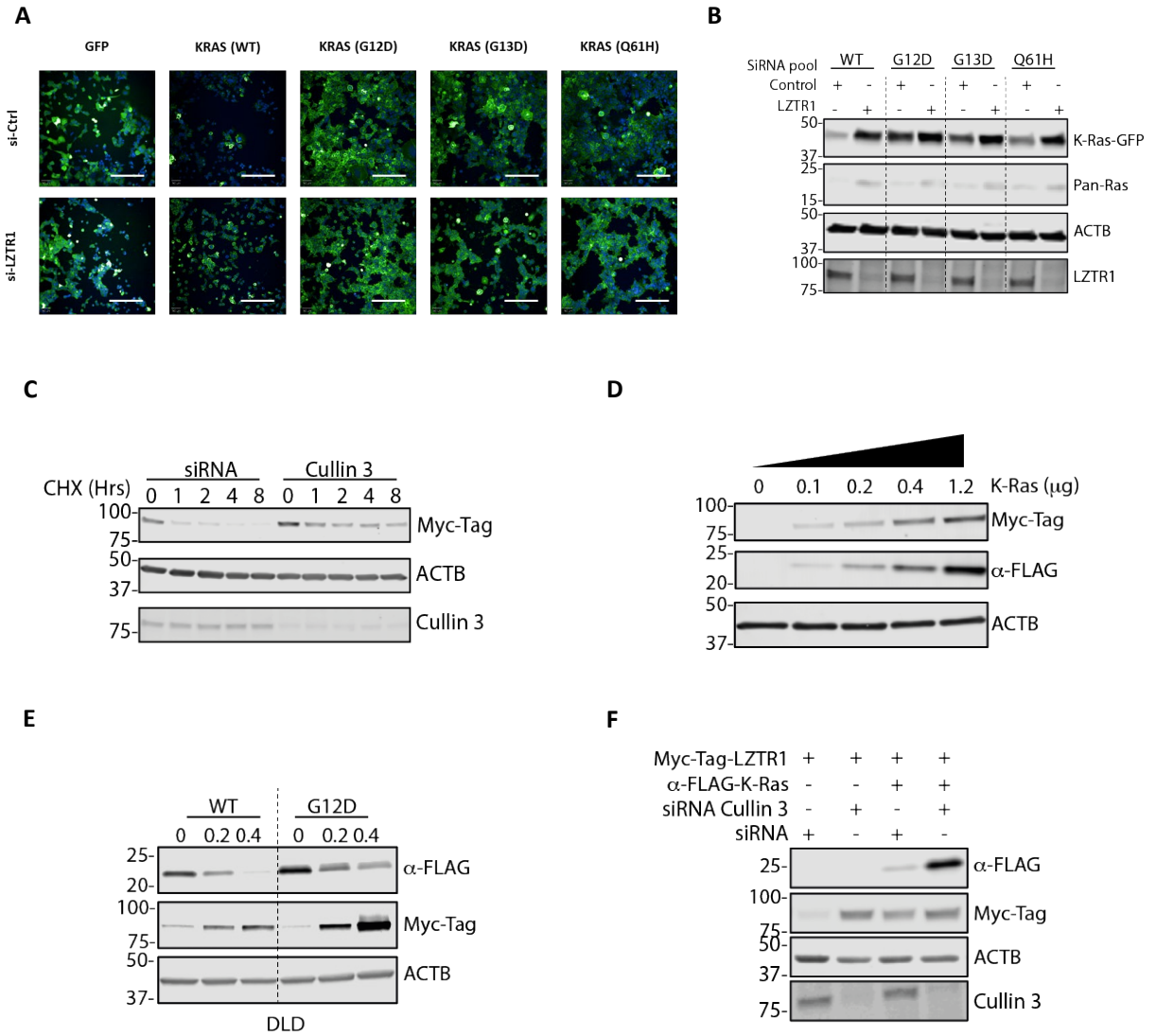
A
GFP
KRAS (WT)
KRAS (G12D)
KRAS (G13D)
KRAS (Q61H)
si-Ctrl
si-LZTR1
B
SiRNA pool
WT
G12D
G13D
Q61H
Control
LZTR1
K-Ras-GFP
Pan-Ras
ACTB
LZTR1
C
siRNA
Cullin 3
CHX (Hrs)
0 1 2 4 8 0 1 2 4 8
Myc-Tag
ACTB
Cullin 3
D
0 0.1 0.2 0.4 1.2 K-Ras (μg)
Myc-Tag
α-FLAG
ACTB
E
WT
G12D
0 0.2 0.4 0 0.2 0.4
α-FLAG
Myc-Tag
ACTB
DLD
F
Myc-Tag-LZTR1
α-FLAG-K-Ras
siRNA Cullin 3
siRNA
α-FLAG
Myc-Tag
ACTB
Cullin 3